Time-Variable Gravity From Satellites

John M. Wahr
Department of Physics and
Cooperative Institute for Research in Environmental Sciences
University of Colorado
Boulder, Colorado 80309-0390

Contents

Abstract

Satellite measurements of time-variable gravity are a new data type, capable of addressing a wide variety of geophysical problems. This subject, in its present form, began with the 2002 launch of GRACE (the Gravity Recovery And Climate Experiment). GRACE has been providing regular monthly estimates of the Earth's gravity field down to scales of several hundred kilometers. Any process that involves enough re-distribution of mass at those temporal and spatial scales is a possible target for GRACE. There are applications for hydrology, oceanography, the cryosphere, and the solid Earth. This chapter summarizes the observational and theoretical framework used to interpret time-variable satellite gravity measurements, and reviews some of the evolving geophysical applications of this technique.

1 Introduction

The Earth's gravity field is a product of its mass distribution; mass both deep within the Earth and at and above its surface. That mass distribution is constantly changing. Tides in the ocean and solid Earth cause large mass variations at 12-hour and 24-hour periods. Atmospheric disturbances associated with synoptic storms, seasonal climatic variations, etc., lead to variations in the distribution of mass in the atmosphere, the ocean, and the water stored on land. Mantle convection causes mass variability throughout the mantle that has large amplitudes compared to those associated with climatic variability, but that generally occurs slowly relative to human timescales.

Because of these and other processes, the Earth's gravity field varies with time. Observations of that variability using either satellites or ground-based instrumentation, can be used to study a wide variety of geophysical processes that involve changes in mass (Dickey *et al.*, 1997). Solid Earth geophysics is not the prime beneficiary of time variable gravity measurements. Instead, most of the time-variable signal comes from the Earth's fluid envelope: the oceans, the atmosphere, the polar ice sheets and continental glaciers, and the storage of water and snow on land. Fluids (water and gasses) are much more mobile than rock.

Solid Earth deformation does have a significant indirect effect on ground-based gravity measurements. A gravimeter on the Earth's surface is sensitive to vertical motion of that surface. When the surface goes up, the gravimeter moves further from the center of the Earth and so it sees a smaller gravitational acceleration. For most solid Earth processes the signal from the vertical displacement of the meter is far larger than the actual gravity change caused by the displaced mass. Thus a surface gravimeter can, in effect, be viewed as a vertical positioning instrument. A satellite, on the other hand, is not fixed to the surface, and so the gravity signals it detects are due entirely to the underlying mass distribution. Thus, satellite gravity provides direct constraints on that mass.

1.1 Non-uniqueness

One serious limitation when interpreting gravity observations is that the inversion of gravity for density is non-unique. There are always an infinite number of possible internal density distributions that can produce the same external gravity field. Even perfect knowledge of the external gravity field would not provide a unique density solution.

As a simple illustration of this non-uniqueness, consider the gravity field outside a sphere. The external gravitational acceleration is $g = MG/r^2$, where M is the total mass of the sphere, G is the gravitational acceleration, and r is the distance to the center of the sphere. This same expression holds whether the mass is uniformly distributed throughout the sphere, or is localized entirely at the outer surface, or has any other radially-dependent distribution. By observing the external gravity field in this case, all that could be learned is the total mass of the sphere and the fact that the internal density is spherically symmetric. The details of how the density is distributed with radius would remain unknown. This non-uniqueness would disappear if the gravity field everywhere inside the sphere were also known. But knowledge of the external field alone is not enough.

This non-uniqueness is a major limitation when interpreting the Earth's static gravity field. For example, Figure 1 shows a map of the Earth's static geoid anomaly, as determined by Lemoine, *et al.*, (1998) from decades of satellite and surface observations. The geoid is the surface of constant potential that coincides with mean sea level over the ocean. The geoid anomaly is the elevation of the geoid above its mean ellipsoidal average. This is a common method of representing the Earth's gravity field, one that emphasizes the long wavelength characteristics of the field. There is a tradeoff between amplitude and depth when using this map to constrain the Earth's time-averaged mass distribution. For example, from this map alone it is not possible to know whether the large red feature over Indonesia is caused by a large positive mass anomaly in the crust, or a much larger mass anomaly deeper in the mantle.

But Figure 1 clearly does contain information about the Earth's internal density. Not every density distribution can produce the same gravity field. The results provide a constraint on a weighted vertical average of the underlying mass anomalies. Static gravity observations are particularly useful when combined with independent information or assumptions about the depth of the density anomaly, or its amplitude, or its spatial pattern.

1.2 Time-variable gravity

Non-uniqueness is much less of an issue for time-varying gravity. Time-varying signals, if they vary rapidly enough, can usually be assumed to come from mass variability at the Earth's surface rather than from deep within the Earth. For example, Figure 2a shows the amplitude of the annual cycle in the geoid as observed from the Gravity Recovery and Climate Experiment (GRACE; see below). It is almost certain that this signal is coming from some combination of the atmosphere, the oceans, and the water/snow/ice stored on or just below the land surface. Few solid Earth processes are likely to vary this rapidly, let alone to show an annual cycle. The only exceptions are the body tide, which can be modeled and removed to an accuracy far better than the accuracy of the GRACE gravity observations; and the response of the solid Earth to the surface mass load. That loading signal, which is typically only a few percent of the signal from the load itself, can be linearly related to the load signal through scale-dependent, well-modeled, proportionality factors (load Love numbers; see below).

Thus, the seasonal mass anomaly can be assumed to be concentrated within a few km of the surface. The inversion for mass anomalies still depends, in principle, on the exact depth of the load. But since the few-km uncertainty in vertical position is much smaller than the horizontal scales of the signals shown in Figure 2a, the corresponding uncertainty in the

amplitude of the inferred mass anomaly is negligible. It is still not possible to tell, without additional information, whether a mass anomaly in a continental region, for example, is in the atmosphere, or in the water and snow on the surface, or in the water stored underground. But at least the total amplitude of the mass anomaly can be determined.

The difficulty with time-variable gravity is that the amplitudes are small. A comparison of Figures 1 and 2a, for example, shows that the annually varying geoid is over 1000 times smaller than the lateral variation in the static field. Most of the Earth's mass, after all, is tied up in it's rocky interior, and remains relatively immobile on human time scales.

Advances in ground-based instrumentation over the last few decades have made it possible to begin to observe time-variable gravity at local scales. Modern, high-precision gravimeters can detect surface displacements caused by solid Earth processes, as well as local gravitational changes caused by variations in the overlying atmosphere and underlying water storage.

But the recovery of large-scale time-varying signals requires satellite measurements. Until the launch of CHAMP (Challenging Microsatellite Payload) in 2001 and, especially, GRACE (Gravity Recovery And Climate Experiment) in 2002, satellite time-variable gravity solutions were based entirely on Satellite Laser Ranging (SLR) observations. The most useful SLR measurements have involved LAGEOS (launched by NASA in 1976) and LAGEOS II (launched jointly by NASA and the Italian Space Agency in 1993). Both satellites are orbiting at 6000 km altitude. They are passives spheres, with outer surfaces covered with corner cube reflectors. A powerful laser on Earth sends a laser pulse up to the satellite, where the light is reflected back to the laser. The round-trip travel time is measured, and so the distance between the laser and the satellite is determined. By monitoring these distances from lasers around the Earth's surface, the satellite's orbital motion is computed. Since the orbital motion is determined by the Earth's gravity field, this allows for global gravity field solutions at regular time intervals. Differences between solutions for different time periods provide estimates of time-variable gravity.

1.3 Changes in the Earth's Oblateness

The first satellite identification of a non-tidal time-varying signal was the recovery of a secular change in the Earth's oblateness. The oblateness is a global-scale component, and is the easiest laterally varying component to detect with a satellite. There are two reasons for this. Let $N(\theta, \phi)$ be the height of the geoid above the Earth's mean spherical surface at latitude θ and eastward longitude ϕ. It is usual to expand N as a sum of Legendre functions (see, e.g., Chao and Gross, 1987):

$$N(\theta,\phi) = a\sum_{l=2}^{\infty}\sum_{m=0}^{l}\tilde{P}_{lm}(\cos\,\theta)(C_{lm}\cos\,(m\phi) + S_{lm}\sin\,(m\phi)) \qquad (1)$$

where a is the radius of the Earth, the $\tilde{P}_{lm}$ are normalized associated Legendre functions, and the C_{lm} and S_{lm} are dimensionless (Stokes) coefficients. Global gravity field solutions are typically provided in the form of a set of Stokes coefficients. The indices l and m in (1) are the degree and order, respectively, of the Legendre function. The horizontal scale of any term in (1) is inversely proportional to the value of l. The half-wavelength of a (l, m) harmonic serves as an approximate representation of this scale, and is roughly (20,000/l) km. Note that the sum over l in (1) begins at $l = 2$. The $l = 0$ term vanishes because

N is defined as the departure from the mean spherical surface; and the $l = 1$ terms vanish by requiring the geoid to be centered about the Earth's center of mass. Thus the $l = 2$ terms are the longest wavelength terms in the series expansion (1). The Earth's oblateness is proportional to C_{20}.

Satellite determinations of gravity are sensitive to the gravity field at the altitude of the satellite, not at the Earth's surface. And the gravitational potential from any (l, m) term in (1) decreases with increasing radius, r, as $(a/r)^{(l+1)}$. Thus, terms with the smallest values of l (i.e. the longest wavelengths) are the least attenuated up at the satellite altitude, and so tend to be the easiest to determine. This tends to favor the recovery of $l = 2$ Stokes coefficients, relative to coefficients with $l > 2$.

At the same time, terms with $m = 0$ are better determined than terms with $m > 0$. This is because an $m = 0$ term does not depend on longitude. For example, Figure 3 shows the patterns of $(l, m) = (2, 0)$ and $= (2, 2)$ terms. Suppose you track a satellite orbiting in the $(2, 0)$ pattern shown in panel (a). As the satellite makes its first orbit, traveling from near the north pole down to near the south pole and back again, it passes through the gravity pattern of red/green/blue shown in the figure, and its orbit gets perturbed accordingly. By the time it begins its second orbit, the Earth has rotated about the polar axis, but because there is no longitude dependence the satellite passes through the same red/green/blue pattern on its second orbit, and so that orbit gets perturbed in the same direction. This happens for every orbit, so the perturbation gradually builds up to large values and is easily seen in the ranging observations. On the other hand, for the $(2, 2)$ pattern in panel (b), every time the satellite begins a new orbit the underlying pattern is different because the Earth's rotation has carried that pattern to the east. Thus, the orbital perturbations do not tend to add constructively and are harder to see.

Early SLR solutions showed a secular increase in C_{20} (Yoder *et al.*, 1983; Rubincam, 1984) which is consistent with a steady migration of mass from low latitudes towards high latitudes. The signal was first interpreted as due to post-glacial rebound (PGR), the Earth's ongoing response to the removal of the ice loads at the end of the last ice age. The areas that lay beneath the ice loads centered over Hudson Bay and over the region around the North and Baltic Seas, are still depressed from the weight of those ancient ice sheets, and they are still gradually uplifting as material deep within the mantle flows in from lower latitudes. In fact, since its first detection, the observed secular change in C_{20} has been used in PGR models to help constrain the Earth's viscosity profile.

More recent SLR solutions give C_{20} trends that are in general agreement with those early estimates (e.g. Cox and Chao *et al.*, 2002; Cheng and Tapley, 2004), though the actual rate tends to be sensitive to the time span of the data and the analysis method used (eg. Benjamin, *et al.*, 2006). A representative C_{20} time series is shown in Figure 4 (data provided by Chris Cox, 2005). There is large seasonal variability, due presumably to a combination of atmospheric pressure variations and variations in the distribution of water in the oceans and on land (eg. Chao and Au, 1991; Dong, *et al.*, 1996; Cheng and Tapley, 1999; Nerem, *et al.*, 2000;). A trend is also clearly evident in the results, and is more pronounced after the data have been low-pass filtered (the red line in Figure 4). But there is also evidence of interannual variability. In particular, notice the anomalous wiggle during 1998-2002 (Cox and Chao, 2002). This feature has been variously explained as the result of climatically driven oscillations in the ocean (Cox and Chao, 2002; Dickey *et al.*, 2002), in the storage of water, snow, and ice on land (Dickey *et al.*, 2002), and as partly the consequence of the

effects of anelasticity on the 18.6-year solid Earth tide (Benjamin, *et al.*, 2006). Whatever its origin, its presence illustrates why solutions for the secular trend depend on the time span.

In addition, it has become increasingly evident in recent years that there could be other processes that involve enough mass transfer between low- and high-latitudes to have a significant impact on the C_{20} trend, and so to confuse the PGR interpretation. The most important of these processes are likely to be changes in ice of the Greenland and Antarctic ice sheets. For example, a rate of Antarctic ice mass loss equivalent to 0.6 mm/yr of global sea level rise averaged over the last 30 years, would cause a C_{20} rate of increase that is about equal in magnitude to the SLR value, though with the opposite sign (eg. Trupin, 1993). If the ice mass trend was even a sizable fraction of this amount, it would have a significant impact on the C_{20} PGR constraint.

These uncertainties arise because knowledge of the single harmonic, C_{20}, is not sufficient to determine the spatial location of the signal. SLR has provided time-variable solutions for a handful of other harmonics (Cheng, *et al.*, 1997; Cheng and Tapley, 1999; Nerem, *et al.*, 2000; Moore, *et al.*, 2005). But there are not nearly enough of these harmonics to give the spatial resolution necessary to confidently address these issues. The basic limitation comes from the high altitude of LAGEOS (6,000 km) and the other SLR satellites. Shorter-scale harmonics in (1) are sufficiently attenuated at those high altitudes that their time-dependence cannot be easily detected. The solution to this problem is to use a satellite in a lower-altitude orbit. That is the motivation for CHAMP (Reigber *et al.*, 2002) and, especially, for GRACE (Tapley *et al.*, 2004a,b).

2 GRACE

The GRACE mission design makes it particularly useful for time-variable gravity studies. Launched jointly by NASA and the German Space Agency (DLR) in March, 2002, GRACE consists of two identical satellites in identical orbits, one following the other by about 220 km. The satellites use microwaves to continually monitor their separation distance to an accuracy of better than 1 micron - about 1/100'th the thickness of a human hair. This distance changes with time as the satellites fly through spatial gradients in the gravity field, and so by monitoring those changes the gravity field can be determined. The satellite altitude is less than 500 km, which makes GRACE considerably more sensitive than SLR to short wavelength terms in the gravity field. The disadvantage of having such a low altitude is that GRACE experiences greater atmospheric drag, which can cause large and unpredictable changes in the inter-satellite distance. To reduce this problem, each GRACE satellite has an on-board accelerometer to measure non-gravitational accelerations. Those measurements are transmitted to the ground where they are used to correct the satellite-to-satellite distance measurements. Each spacecraft also has an on-board GPS receiver, used to determine the orbital motion of each spacecraft in the global GPS reference frame and to improve the gravity field solutions at global-scale wavelengths.

2.1 Gravity Solutions

GRACE transmits raw science instrument and satellite housekeeping data to the ground, where they are transformed into physically meaningful quantities: e.g. satellite-to-satellite

distances, non-gravitational accelerations, spacecraft attitudes, etc.. These quantities, called Level-1 data, are made publically available and can be used to construct gravity field solutions. Since few users have the capability of constructing their own gravity solutions from these data, the GRACE Project does that as well, and makes those solutions, referred to as Level-2 data, available on the web.

The Level-2 gravity products consist of complete sets of harmonic (Stokes) coefficients (1) out to some maximum degree and order (typically $l_{\max} = 120$), averaged over monthly intervals. Larger sets of coefficients averaged over longer time intervals are also provided to represent the static field. Harmonic coefficients can be used to generate geoid, gravity, or mass solutions at individual locations, or averaged over specific regions, as described below. Level-2 products are generated at several Project-related processing centers (i.e. the Center for Space Research at the University of Texas, GeoForschungsZentrum in Potsdam, Germany, and the Jet Propulsion Laboratory), and each of these products is made available to users.

Harmonic solutions are traditional in satellite geodesy. Harmonics help with the problem of upward and downward continuing the gravity field between the surface and the satellite altitude, during the solution process. Specifically, the gravitational potential caused by any (l, m) term in (1) has a particularly simple radial dependence, decreasing with increasing radius, r, as $(a/r)^{(l+1)}$.

Nevertheless, users sometimes generate non-harmonic solutions directly from the Level-1 data. Various methods have been derived for doing this, most of which involve partitioning the time-variable surface mass field into small regions, and using the Level-1 data to directly determine the mass in each of those regions. For example, the first and second time-derivatives of the satellite-to-satellite distance are the along-track differences in velocity and acceleration of the two satellites. These can be used to determine the along-track gradients of the gravitational potential and acceleration, respectively. These gradients can then be fit to upward-continued mass signals from specific regions, to determine the amplitudes of those mass signals (see, for example, Jekeli, 1999; Visser, *et al.*, 2003; Han, *et al.*, 2005a, 2006a; Schmidt, *et al.*, 2006a)

Another approach involves the construction of "mascon" solutions (e.g. Rowlands, *et al.*, 2005; Watkins and Yuan, 2006; Yuan and Watkins, 2006). Mascons, in this context, are mass anomalies spread uniformly over either regular- (usually rectangular) or irregular-shaped blocks (Luthcke, *et al.*, 2006) at the Earth's surface. Each such mass anomaly has an overall scale factor, which is determined from the Level-1 data.

These alternative methods are usually designed to estimate regional mass anomalies, rather than to generate results everywhere over the globe. They thus often ingest only those Level-1 data that are acquired when the satellites are over the region of interest. This tends to reduce a problem common to global harmonic solutions, in which errors, either in the satellite measurements or in the geophysical background models, that affect the satellites in one region, end up leaking into the gravity field solutions in distant regions.

2.2 Using the harmonic solutions to solve for mass

Most users do not have the resources to process Level-1 data, and rely instead on the standard Level-2 gravity field products: the harmonic solutions. For most applications the gravity field itself is not of direct interest. Instead, it is usually the mass distribution causing the

gravity field that is the desired quantity. Here, we describe how that mass distribution can be inferred from the harmonic gravity solutions. We focus specifically on the time-variable components of the gravity and mass fields. The methods described here are described in more detail in Section 2.1 of Wahr *et al.*, (1998) (see, also, Chao and Gross, 1987).

The time-variable component of the gravity field is obtained by removing the long-term mean of the Stokes coefficients from each monthly value. The mean can be obtained from one of the static fields available as Level-2 products. Or, perhaps more usefully, it can be estimated by simply constructing the average of all the monthly fields used in the analysis. The reason for removing the mean field is that it is dominated by the static density distribution inside the solid Earth. It thus has no bearing on attempts to learn about, say, the distribution of water stored on land or in the ocean. Removing the static field, though, means that all contributions from the mean stored water are also removed. Thus, only the time-variable component of the water storage can be recovered.

The time-variable gravity field is then used to solve for the time-variable mass field. This solution is non-unique, as described in the Introduction. Let ΔC_{lm} and ΔS_{lm}, be the time-variable components of the (l, m) Stokes coefficients for some month. Let $\Delta\rho(r, \theta, \phi)$ be the density redistribution that causes this time-dependent change in gravity. Then:

$$\left\{ \begin{array}{c} \Delta C_{lm} \\ \Delta S_{lm} \end{array} \right\} = \frac{3}{4\pi a \rho_{\rm ave}(2l+1)} \int \Delta\rho(r,\theta,\phi) \left(\frac{r}{a}\right)^{l+2} \tilde{P}_{lm}(\cos\,\theta) \left\{ \begin{array}{c} \cos\,(m\phi) \\ \sin\,(m\phi) \end{array} \right\} \sin\,\theta\, d\theta\, d\phi\, dr \tag{2}$$

where ρ_{ave} is the average density of the Earth (= 5517 kg/m^3).

Suppose the density is expanded as a sum of Legendre functions:

$$\Delta\rho(r,\theta,\phi) = \sum_{l=0}^{\infty} \sum_{m=0}^{l} \tilde{P}_{lm}(\cos\theta)(\Delta\rho^c_{lm}(r)\cos\,(m\phi) + \Delta\rho^s_{lm}(r)\sin\,(m\phi)) \tag{3}$$

Using (3) in (2), and employing orthogonality relations for Legendre functions, (2) reduces to

$$\left\{ \begin{array}{c} \Delta C_{lm} \\ \Delta S_{lm} \end{array} \right\} = \frac{3}{a\rho_{\rm ave}(2l+1)} \int \left\{ \begin{array}{c} \Delta\rho^c_{lm}(r) \\ \Delta\rho^s_{lm}(r) \end{array} \right\} \left(\frac{r}{a}\right)^{l+2} dr \tag{4}$$

This result, (4), can be used to place constraints on $\Delta\rho(r, \theta, \phi)$ from measurements of ΔC_{lm} and ΔS_{lm}. The non-uniqueness is evident here in the fact that ΔC_{lm} and ΔS_{lm} provide information only on the radial integral of the density coefficients. There is no way of determining how the density depends on depth within the Earth.

Suppose, though, we have reason to believe the observed ΔC_{lm} and ΔS_{lm} are caused by mass variability concentrated within a thin layer of thickness H near the Earth's surface; a layer containing those regions of the atmosphere, oceans, ice sheets, and land water storage that are subject to significant mass fluctuations. H, in this case, would be mostly determined by the thickness of the atmosphere, and is of the order of 10 km. If H is thin compared to the horizontal resolution of the observations, then the the amplitude of the density anomaly can be uniquely determined, as follows.

Suppose the observed gravity field is accurate enough to resolve gravity anomalies down to scales of R km. That means the ΔC_{lm} and ΔS_{lm}'s contain useful information for values of l up to $l_{\rm max} = 20000/R$. At present GRACE has a typical resolution of ~750 km, though

resolutions as small as ∼300 km can be obtained by employing post-processing methods (Swenson and Wahr, 2006a). Thus, at present $l_{\max} \sim 65$. Suppose H is thin enough that

$$(l_{\max} + 2)H/a << 1 \quad . \tag{5}$$

Then, $(r/a)^{l+2} \approx 1$ for all usable values of l, and so (2) reduces to

$$\left\{ \begin{array}{c} \Delta C_{lm}^{\text{surf mass}} \\ \Delta S_{lm}^{\text{surf mass}} \end{array} \right\} = \frac{3}{4\pi a \rho_{ave}(2l+1)} \int \Delta\sigma(\theta,\phi)\, \tilde{P}_{lm}(\cos\theta) \left\{ \begin{array}{c} \cos(m\phi) \\ \sin(m\phi) \end{array} \right\} \sin\theta\, d\theta\, d\phi \tag{6}$$

where $\Delta\sigma$ is the change in surface density (i.e., mass/area), defined as the radial integral of $\Delta\rho$ through the surface layer:

$$\Delta\sigma(\theta,\phi) = \int_{\text{thin layer}} \Delta\rho(r,\theta,\phi)dr \tag{7}$$

The assumption that the density anomaly is concentrated within this thin layer is incorrect. Any change in mass load at the surface will induce deformation within the solid Earth, leading to a density anomaly at depth as well. The gravity signal caused by these solid Earth mass anomalies is typically a few percent of the gravity anomaly caused by the surface mass, and fortunately can be easily represented in terms of load Love numbers, k_l (see, e.g., Farrell, 1972; Chao, 1994, equation (6)). Specifically, if $\Delta C_{lm}^{\text{solid Earth}}$ and $\Delta S_{lm}^{\text{solid Earth}}$ represent the contributions to the gravity field from the load-induced deformation in the solid Earth, then

$$\left\{ \begin{array}{c} \Delta C_{lm}^{\text{solid Earth}} \\ \Delta S_{lm}^{\text{solid Earth}} \end{array} \right\} \;=\; k_l \left\{ \begin{array}{c} \Delta C_{lm}^{\text{surf mass}} \\ \Delta S_{lm}^{\text{surf mass}} \end{array} \right\} \tag{8}$$

Thus, the total dependence of the Stokes coefficients on the surface mass density is

$$\left\{ \begin{array}{c} \Delta C_{lm} \\ \Delta S_{lm} \end{array} \right\} = \frac{3}{4\pi a \rho_{ave}} \frac{1+k_l}{(2l+1)} \int \Delta\sigma(\theta,\phi)\, \tilde{P}_{lm}(\cos\theta) \left\{ \begin{array}{c} \cos(m\phi) \\ \sin(m\phi) \end{array} \right\} \sin\theta\, d\theta\, d\phi \tag{9}$$

By expanding $\Delta\sigma(\theta,\phi)$ as a sum of Legendre coefficients, similar to the expansion shown in (3) for $\Delta\rho$, and using the orthogonality of the Legendre functions to obtain a result similar to (4), we find:

$$\Delta\sigma(\theta,\phi) = \frac{a\rho_{ave}}{3} \sum_{l=0}^{\infty} \sum_{m=0}^{l} \frac{2l+1}{1+k_l} \tilde{P}_{lm}(\cos\,\theta)(\Delta C_{lm}\cos(m\phi) + \Delta S_{lm}\sin(m\phi)) \tag{10}$$

The results above assume the surface layer is thin enough that (5) is valid. If we assume that $l_{\max} = 65$, and that the layer includes the atmosphere so that $H \sim 10$ km, then (5) is violated at about the 10% level. This is a large enough inaccuracy that it might be important, for some applications, to include the radial distribution of atmospheric density fluctuations. Methods of doing this are described in Swenson and Wahr (2002a). Mass variations in the oceans and in the water stored on land occur almost entirely within 1 km of the surface, and usually much closer to the surface than that. For a 1 km thick layer and $l_{\max} = 65$, (5) is accurate to ∼1%, which is easily good enough for oceanographic and hydrological applications.

2.3 Love numbers

The use of (10) to recover surface mass requires knowledge of the load Love numbers k_l. As a guide, one set of results for those Love numbers is given in Table 1 (D. Han, personal communication, 1998) for a few values of l up to 200. These results are computed as described by Han and Wahr (1995), using Earth structural parameters from the Preliminary Reference Earth Model (PREM) of Dziewonski and Anderson (1981). Results for other values of $l < 200$ can be obtained by linear interpolation of the Table 1 results. Linearly interpolating the Table 1 results, instead of using exact results, introduces errors of less than 0.05% for all $l < 200$.

These results for k_l do not include anelastic effects. Those effects increase with increasing period but are apt to be negligible for our applications. For example, *Wahr and Bergen* (1986) concluded that at an annual period the anelastic effects on the $l = 2$ body tide Love number, $k_2^{\rm body}$, would probably be less than 2%, corresponding to an effect on $(1 + k_2^{\rm body})$ of less than 1% . Even allowing for larger effects at longer periods, and perhaps a somewhat greater effect for load Love numbers than for body tide Love numbers (since load Love numbers are more sensitive to upper mantle structure where the anelastic effects could be larger), we tentatively conclude that anelasticity would not perturb the results for $(1 + k_l)$ by more than a few percent.

The Love numbers in (10) with $l = 0$ and $l = 1$ require discussion. The $l = 0$ term is proportional to the total mass of the Earth where "the Earth" includes not only the solid Earth, but also its fluid envelope (the oceans, atmosphere, etc.). This total mass does not change with time, and so ΔC_{00} from GRACE can be assumed to vanish. Suppose, though, the objective is to use (10) to find the surface mass contribution from just one component of the surface mass: say, the ocean, for example. The total mass of the ocean need not be constant, due to exchange of water with the atmosphere or the land surface. So the oceanic contributions to $\Delta\hat{C}_{00}$ need not vanish. But this nonzero $\Delta\hat{C}_{00}$ will not induce an $l = 0$ response in the solid Earth: i.e., the load does not cause a change in the total solid Earth mass. Thus $k_0 = 0$.

The $l = 1$ terms are proportional to the position of the Earth's center of mass relative to the center of the coordinate system and so depend on how the coordinate system is chosen. One possibility is to choose a system where the origin always coincides with the Earth's instantaneous center of mass. In that case all $l = 1$ terms in the geoid are zero by definition, and so the GRACE results for $\Delta C_{lm} = \Delta S_{lm} = 0$ for all $l = 1$. This is the coordinate system used for the geoid representation shown in (1). Again, the $l = 1$ coefficients for an individual component of the total surface mass need not vanish. Redistribution of mass in the ocean, for example, can change the center of mass of the ocean. But that will induce a change in the center of mass of the solid Earth, so that the center of mass of the ocean + solid Earth remains fixed. So, for this choice of coordinate system, $k_{l=1} = -1$.

Another possibility is to define the coordinate system so that its origin coincides with the center of figure of the Earth's solid outer surface. That is the most sensible way of defining the origin when recovering the Earth's time-variable mass distribution, since hydrological, oceanographic, and atmospheric models are invariably constructed in a system fixed to the Earth's surface. In that case the $l = 1$ GRACE results for $\Delta C_{lm} = \Delta S_{lm}$ need not vanish, and the Love number $k_{l=1}$ is defined so that the $l = 1$ terms in (10) describe the offset between [the center of mass of the surface mass + deformed solid Earth] and [the center of

figure of the deformed solid Earth surface]. It is shown by Trupin *et al.* (1992; equation (10)) that for this coordinate system $k_{l=1} = -(h_{l=1} + 2\ell_{l=1})/3$, where $h_{l=1}$ and $\ell_{l=1}$ are the $l = 1$ displacement Love numbers when the origin is the center of mass of the deformed solid Earth. For this choice of origin, the numerical value of $k_{l=1} = -(h_{l=1} + 2\ell_{l=1})/3$ is given in Table 1.

2.4 Spatial averaging

Equation (10) is the starting point for using GRACE estimates of ΔC_{lm} and ΔS_{lm} to recover changes in surface mass density. Because the errors in the GRACE results become large for large l (i.e. short scales), and because terms with large l values can make important contributions to the sum in (10) (note the $2l + 1$ factor in the numerator of (10)), the use of (10) as written can lead to highly inaccurate results.

To obtain accurate results it is necessary to somehow reduce the large-l contributions to the sum (10). This involves the insertion of some additional multiplicative factor into (10), that is small for large values of l. Any such modification means that the sum will no longer be an exact representation of the surface mass at (θ, ϕ). Since most applications require the surface mass in the spatial domain, it is useful to choose a multiplicative factor in such a way that the sum still has some meaningful connection to the spatially dependent surface mass. Any multiplicative factor applied in the spectral (l, m) domain is equivalent to convolving with some corresponding weighting function in the spatial domain. The problem is to choose a factor that reduces the errors, but that keeps the weighting function localized. The issues are similar to those encountered when designing filters for time series analysis, where the generic problem is to construct a filter that removes noise but that still provides a meaningful estimate of the true signal in the time domain.

Various methods have been used for improving the GRACE mass estimates in this way, though most of them are similar to one another (Wahr, *et al.*, 1998; Swenson and Wahr, 2002b; Swenson *et al.*, 2003; Seo and Wilson, 2005; Chen *et al.*, 2006a; Han *et al.*, 2005b). These methods fall into one of two categories: smoothing the surface mass results, or averaging over specific regions.

2.4.1 Smoothing

The simplest way of modifying (10) to obtain accurate results, is to introduce degree-dependent weighting factors W_l into the sum, so that

$$\overline{\Delta\sigma}(\theta,\phi) = \frac{a\rho_{\rm ave}}{3}\sum_{l,m}\frac{2l+1}{1+k_l}W_l\tilde{P}_{lm}(\cos\,\theta)\,[\Delta C_{lm}\cos\,(m\phi) + \Delta S_{lm}\sin\,(m\phi)] \qquad (11)$$

$\overline{\Delta\sigma}$ then represents a smoothed version of the surface mass anomaly, given by

$$\overline{\Delta\sigma}(\theta,\phi) = \int \sin\,\theta'\,d\theta'\,d\phi'\,\Delta\sigma(\theta',\phi')\,W(\alpha) \qquad (12)$$

where α is the angle between (θ, ϕ) and (θ', ϕ'), and $W(\alpha)$ is a smoothing function corresponding to the choice of the W_l's:

$$W(\alpha) \;=\; \frac{1}{4\pi}\sum_l \sqrt{2l+1}\,W_l\tilde{P}_{l0}(\alpha) \quad . \qquad (13)$$

One obvious way of smoothing is simply to truncate the sum over l so that the inaccurate coefficients at large-l are not included. This is equivalent to choosing $W_l = 1$ for values of l less than some $l_{\max}$, and $W_l = 0$ for $l \geq l_{\max}$. This approach can, indeed, give accurate results for the sum if $l_{\max}$ is chosen to be small enough. The disadvantage of using this step-function weighting, is that the equivalent convolution function, $W(\alpha)$, "rings" in the spatial domain (see panels (a) and (b) in Figure 5)). The results for $\overline{\Delta\sigma}$ in this case are an average not only of the true values of $\Delta\sigma$ at points close to (θ, ϕ), but also of $\Delta\sigma$ values at points all around the globe, and where the smoothing function has an oscillating sign.

This ringing can be avoided by choosing W_l to decrease smoothly with l. A convenient choice of smoothing coefficients (see, e.g., Wahr *et al.*, 1998) are the Gaussian values developed by Jekeli (1981) to improve estimates of the Earth's gravity field. Those coefficients can be found using the recursion relations

$$\begin{aligned} W_0 &= 1 \\ W_1 &= \frac{1 + e^{-2b}}{1 - e^{-2b}} - \frac{1}{b} \\ W_{l+1} &= -\frac{2l+1}{b} W_l + W_{l-1} \end{aligned} \tag{14}$$

These coefficients correspond to to a smoothing function

$$W(\alpha) = \frac{b \exp\left[-b(1 - \cos\,\alpha)\right]}{1 - e^{-2b}} \tag{15}$$

where

$$b = \frac{\ln(2)}{(1 - \cos\,(r/a))} \tag{16}$$

and r is the distance on the Earth's surface at which W has decreased to 1/2 its value at $\alpha = 0$ (the distance on the Earth's surface $= a\alpha$). We will refer to r as the smoothing radius. As an example, panels (c) and (d) Figure 5 show $W(\alpha)$ and W_l for $r = 400$ km. Note that the convolution function, $W(\alpha)$, decreases smoothly to zero at large angular distances, and does not oscillate. In practice, there will always be some oscillation, since no satellite gravity field model will ever provide Stokes coefficients out to infinite degree. But as long as the W_l are small out at the value of the maximum degree in the gravity model, the ringing is minimal.

The annual amplitudes shown in Figure 2b are obtained by applying a Gaussian smoothing function with a 750-km radius, to monthly GRACE mass solutions between the spring of 2002 and the spring of 2006. For comparison, the top panel of Figure 6 shows results for a single month (after the temporal mean has been subtracted) for a 400 km radius. Note the notably increased noise for the shorter averaging radius. This occurs because the high-degree terms in (10) are not attenuated as effectively for shorter smoothing radii. The disadvantage of using longer smoothing radii is that the results in the spatial domain are less able to pick up short-scale structure in the mass anomalies.

The results shown in the top panel of Figure 6 suggest that 400-km resolution is beyond the current capabilities of GRACE. Note that the noise seems to be oriented in north-south stripes. This is a familiar characteristic of GRACE gravity solutions; and is not found,

for example, in SLR gravity fields. It occurs because the GRACE satellites measure gravity gradients along-track, and since the GRACE inclination is 89^o, the tracks are oriented north-south. Thus there is little east-west sensitivity and so any errors in the measurements or in the processing, tend to be put into east-west gradients. Post-processing methods can be used to remove those stripes. The bottom panel of Figure 6 shows results for the same 400-km smoothing radius as the top panel, but after applying the post-processing method described in Swenson and Wahr (2006a). Simulations show that this method reduces stripes with only minimal impact on real signal. Note that the stripes in the bottom panel are, indeed, greatly reduced, and that features that look like true signal are now clearly evident.

2.4.2 Regional averaging

Many applications require estimates of mass variability for specific regions; for example, estimating changes in mass of the Antarctic ice sheet, or changes in water storage in the Mississippi River basin. These sorts of problems are better addressed by constructing specific averaging functions optimized for those regions, than by employing the sort of generic smoothing functions described above.

For example, an exact regional average would take the form

$$\Delta\sigma_{region} = \frac{1}{\Omega_{region}} \int \Delta\sigma(\theta,\phi)\vartheta(\theta,\phi)\, sin\theta d\theta\, d\phi \tag{17}$$

where Ω_{region} is the angular area of the region of interest, and where

$$\vartheta(\theta,\phi) \;= \begin{cases} 0 \text{ outside the basin} \\ 1 \text{ inside the basin} \end{cases} . \tag{18}$$

The result (17) can be expressed as a sum of Stokes coefficients:

$$\Delta\sigma_{region} = \frac{a\ \rho_{ave}}{3\,\Omega_{region}} \sum_{l=0}^{\infty}\sum_{m=0}^{l} \frac{(2l+1)}{(1+k_l)} (\vartheta^c_{lm}\Delta C_{lm} + \vartheta^s_{lm}\Delta S_{lm}) \ , \tag{19}$$

where ϑ^c_{lm} and ϑ^s_{lm} are the harmonic coefficients of $\vartheta(\theta,\phi)$. Since the averaging function, $\vartheta(\theta,\phi)$ in this case, changes abruptly from 1 to 0 along the edge of the region, it has power at short spatial scales. Thus ϑ^c_{lm} and ϑ^s_{lm} can be relatively large at high degrees, and so this estimate of $\Delta\sigma_{region}$ can be inaccurate.

The way around this problem is to smooth the averaging function, so that it is close to 1 inside the region and close to 0 outside, and varies smoothly between 0 and 1 along the edges. We replace (17) with:

$$\overline{\Delta\sigma}_{region} = \frac{1}{\Omega_{region}} \int \Delta\sigma(\theta,\phi)\overline{W}(\theta,\phi)\, sin\theta d\theta\, d\phi \tag{20}$$

where the averaging function

$$\overline{W}(\theta,\phi) = \frac{1}{4\pi}\sum_{lm} \tilde{P}_{lm}(cos\theta)\{W^c_{lm}cos(m\phi) + W^s_{lm}sin(m\phi)\} \ , \tag{21}$$

is chosen to closely approximate $\vartheta(\theta,\phi)$, but to vary smoothly enough that its expansion coefficients W^c_{lm} and W^c_{lm} are small for large values of l. In that case, the spectral equivalent to (20),

$$\overline{\Delta\sigma}_{region} = \sum_{l,m} \frac{a\ \rho_{ave}}{3\Omega_{region}} \frac{(2l+1)}{(1+k_l)} \left(W^c_{lm}\Delta C_{lm} + W^s_{lm}\Delta S_{lm}\right) , \tag{22}$$

will be both reasonably representative of the true regional average, and reasonably accurate. Methods of optimizing the choice of $\overline{W}(\theta,\phi)$, based on estimates of the true signal characteristics, are described by Swenson and Wahr (2002b) and Swenson *et al.* (2003) (see, also, Seo and Wilson, 2005). In general, the larger the region the more accurate the results. Examples of optimal averaging functions for Antarctica and for the Mississippi Basin are shown in Figure 7. Note that in both cases the averaging function is smaller than 1 inside the region, and remains larger than 0 for some distance outside the region.

2.5 Estimating errors and accounting for leakage

Errors in a surface mass estimate separate into two categories: those due to errors in the Stokes coefficients, and those caused by leakage from other signals. Errors in the Stokes coefficients can be caused by instrumental, data processing, or aliasing errors. Temporal aliasing errors in the GRACE monthly gravity fields are caused by short-period (sub-monthly) variations in gravity. The satellite does not monitor the entire global field continually during a month, but samples the gravity field only along its orbital path. Infrequent sampling of a short-period signal can cause aliasing into the monthly averages. The best way to reduce these aliasing errors is to independently model and remove the effects of short-period gravity variations before constructing monthly averages. For GRACE, this means modeling and removing the effects of solid Earth and ocean tides, of atmospheric mass variability over land (using global, gridded atmospheric fields available from the European Centre for Medium-Range Weather Forecasts: ECMWF), and of short period variations in ocean bottom pressure (using an ocean general circulation model). Errors in any of those models cause aliasing errors in the monthly gravity field solutions (Knudsen and Andersen, 2002; Song and Zlotnicki, 2004; Han *et al.*, 2004, 2005c; Thompson *et al.*, 2004; Schrama, 2004; Ray and Luthcke, 2006).

To see how errors in the Stokes coefficients from any source (i.e. instrumental, processing, aliasing), map into errors in a mass estimate, let δC_{lm} and δS_{lm} be the root-mean-square (rms) errors in the Stokes coefficients. The smoothed estimates (11) and the regional averages (22) are both of the form

$$\sigma = \sum_{l,m} \left[F^m_l \Delta C_{lm} + G^m_l \Delta S_{lm}\right] \quad . \tag{23}$$

Suppose the errors in the different Stokes coefficients are uncorrelated with one another. Then the corresponding rms error in σ would be

$$\delta\sigma = \sqrt{\sum_{l,m} \left(F^2_{lm}\delta C^2_{lm} + G^2_{lm}\delta S^2_{lm}\right)} \quad . \tag{24}$$

The errors in different Stokes coefficients are unlikely to be uncorrelated. For GRACE, those correlations are responsible for the stripes evident in the top panel of Figure 6. Knowledge of the full error covariance matrix can improve the estimate of $\delta\sigma$. But even without

the full covariance, (24) provides a reasonable first approximation for $\delta\sigma$, if δC_{lm} and δS_{lm} can be estimated.

To understand leakage errors, consider an application where the goal is to use the Stokes coefficients to assess a regional water storage model. For example, suppose a surface mass average of the form (22) is constructed and interpreted as an estimate of water storage variability in some chosen river basin. Leakage errors are the contributions to (22) caused by gravity signals from outside the basin.

These leakage errors can come from time variable mass anomalies either vertically above or below the river basin, or from mass anomalies off to the side of the basin. Signals above or below would come from the overlying atmosphere or the underlying solid Earth, and can not be separated from the river basin signal no matter how complete and accurate the gravity field estimation. This is a consequence of the non-uniqueness of gravity-based inversions for density, as described above. The only recourse is to independently model and remove the atmospheric and solid Earth signals. Any inaccuracy in those models is thus a source of errors for the hydrology estimates (Velicogna *et al.*, 2001).

Leakage from mass anomalies off to the side, in neighboring river basins for example, can be minimized using a weighting function that is as localized as possible to the river basin of interest. As described above, though, an averaging function should usually be smoother than the basin function to provide an accurate estimate.

For some applications, this horizontal leakage is not an issue. For example, suppose the objective is to compare the satellite estimates of σ for the Mississippi River basin, with the output of a hydrology model. The leakage into the satellite estimate will come mainly from the river basins that border the Mississippi basin. If the same averaging function is applied to the model output, then both will be subject to the same leakage. The model-satellite comparison will then actually be a comparison over a somewhat broader region than just the Mississippi basin, but they will both be affected by leakage in the same way.

But for many applications the goal is to estimate mass variability within a specific region with no contamination from regions outside. In that case, leakage is an inescapable source of error. The only way to estimate the likely impact of that error is to apply the averaging function to simulated data. This sort of problem commonly arises in time series analysis. Our averaging process is basically a low pass filter. A high pass filter not only removes high frequencies, but also reduces the low frequency signal; i.e. each filter has a characteristic gain function. The effects of the gain function must be determined and removed from the filtered data, in order to estimate the true low frequency signal in the time domain.

The examples shown in Figure 7, i.e. the Mississippi basin and Antarctica, illustrate two types of situations. For the Mississippi, the averaging function will downweight the true Mississippi signal, since the averaging function is smaller than 1 over the entire basin. In effect, the averaging function replaces some of the signal located inside the Mississippi basin, with signals located outside in neighboring basins. The amount of leakage thus depends on whether the external hydrology signal does or does not look like the internal signal. It basically depends on a comparison between the correlation length of the hydrology signal (which tends to be controlled by the scale length of the precipitation) and the resolution of the averaging kernel (which is usually is chosen based on the resolution of the gravity field). For a reasonably homogeneous region like this portion of the interior United States, the signal just outside the basin is similar enough to the signal just inside, that the leakage from the averaging kernel shown in Figure 7 is not severe. Nonetheless, the leakage is non-zero,

and should be estimated using hydrology model output.

For Antarctica, the extension of the averaging function over the ocean means that some Antarctic signal is being replaced by ocean signal. There is likely to be no correlation at all between the Antarctic and ocean signals. For example, suppose the object is to determine the linear trend in Antarctic mass over some multi-year period. It is probable that there would be little or no multi-year trend over the ocean. So the averaging process under-represents the contribution from the trend in Antarctic mass, and replaces it with a negligible trend from the ocean. This can lead to serious underestimates of the Antarctic mass trend. The situation is similar for any region where the signal of interest is much larger than the signal in surrounding areas. Again, the only way to assess and correct for this effect is to apply the averaging function to simulated data for the Antarctic ice sheet and the surrounding ocean. Velicogna and Wahr (2006a), for example, found that the Antarctic averaging kernel shown in Figure 7 underestimates the true Antarctic signal by about 35-40%. This correction, which Velicogna and Wahr refer to as scaling, is equivalent to correcting for the gain of the spatial filter represented by W_{lm}^c and W_{lm}^s in (22).

In principle, the sum in (22) should include all l in the range $0 \leq l \leq \infty$. In practice, the sum for GRACE is limited to $2 \leq l \leq l_{max}$, where l_{max} can be no larger than the maximum degree of the GRACE fields. The truncation to $l \leq l_{max}$ causes ringing: sensitivity to mass variability well outside the region of interest; though this sensitivity is weak if l_{max} is large. The restriction to $l \geq 2$ arises because GRACE does not recover $l = 0$, 1 coefficients. The $l = 0$ coefficient is proportional to the Earth's total mass. Since that mass remains constant, $\Delta C_{00} = 0$ is a reasonable assumption. But the omission of $l = 1$ terms in (22) has the potential of degrading estimates of $\overline{\Delta\sigma}_{region}$. Those terms are proportional to the displacement of the geocenter (the offset between the Earth's center of mass and the center of figure of the surface), and are particularly affected by the seasonal transfer of water between the continents and the ocean. Their omission from (22) means, in effect, that the averaging function has a small-amplitude tail that extends around the globe, causing distant signals to leak into $\overline{\Delta\sigma}_{region}$. This leakage can be estimated either by using independent estimates of geocenter motion from other techniques (i.e. SLR, or GPS), or by using hydrological and oceanographic models.

3 Applications

Time-variable satellite gravity measurements can be used to address a wide variety of problems, from across a broad spectrum of the Earth sciences. Any geophysical process that causes a significant redistribution of mass over scales of hundreds of kilometers is a possible target.

3.1 Hydrology

The largest-amplitude and most varied time-dependent signals are related to water storage variability on land. Figure 2b, for example, shows that the annually varying signals on land are much larger than those in the ocean. When water is placed on land a sizable fraction often stays there for some time, either infiltrating into the soil or remaining on the surface as water or snow. But when a parcel of water is placed on the ocean its natural tendency is to

flow away. Note that the the largest features evident in Figure 2b are easily recognized: e.g. heavy-rainfall regions near the equator, the strong monsoon in southeast Asia, the seasonal snow cycle in Eurasia and northern North America. A higher-resolution (300 km Gaussian smoothing) example is shown in Figure 8. Features clearly evident include the rain forest in Central America, the heavy mountain snows that stretch from southern Alaska down through the Central Rocky Mountains, the desert region of the Southwest United States, the region of high precipitation running from the lower Mississippi Basin up through Kentucky, and the high precipitation region along the upper Saint Lawrence River.

Time-variable gravity measurements are sensitive to the total water storage integrated through the entire water column (see (7)). This includes water and snow on the surface, and water in both the soil and sub-soil layers. The measurements cannot distinguish between these stores, but can recover only the sum. This hydrological product is unique, both in its sensitivity to sub-soil water storage and in its ability to recover results at large spatial scales. Other types of satellite-based instruments, either already on orbit or still in the planning stage, can detect water stored within the upper few cm of the soil, or can monitor surface water. But time-variable gravity missions provide the only available means of monitoring deeper water storage from space. Ground-based observations from such things as soil moisture probes and the monitoring of well levels, can provide information on sub-surface storage at individual points. But probably no region in the world has a dense enough observational network to provide total water storage at scales of a few hundred km with the accuracy of GRACE.

Comparing with land surface models. Water storage estimates obtained from time-variable gravity are of potential value both as stand-alone quantities and when used in combination with other data types. As an end product they can be compared with the total water storage predicted by land surface models, to help assess and improve those models (Ramillien *et al.*, 2005; Andersen and Hinderer, 2005; Andersen *et al.*, 2005; Niu and Yang, 2006; Nakaegawa, 2006; Swenson and Milly, 2006; Neumeyer *et al.*, 2006; Seo *et al.*, 2006; Schmidt *et al.*, 2006b; Hinderer *et al.*, 2006; Frappart *et al.*, 2006); and with soil moisture, ground water, and/or snow mass measurements to help validate and understand those measurements (Swenson *et al.*, 2006; Frappart *et al.*, 2006; Yeh *et al.*, 2006). For example, Figure 9 (Sean Swenson, personal communication) shows comparisons between GRACE water storage estimates and those predicted by the GLDAS/Noah water storage model (Rodell, *et al.*, 2004a), for three river basins. The GRACE error bars are defined so that if the disagreement for any month is larger than the error bars, we can be 68.3% confident that it is the model that is in error (Wahr *et al.*, 2006). The agreement is excellent for the Mississippi, which is reassuring given the high density of observations used to improve the atmospheric forcing fields in that region. For the Amazon the phase of the model tends to slightly lead the phase of GRACE; and for the Yenisey (in northern Siberia) the phase disagreement is more pronounced, with the model losing mass perhaps a couple months too early in the early springs of 2003 and 2004. Comparisons like these can provide an indication of where model improvements are necessary. Eventually, gravity-based water storage estimates could even be assimilated directly into the hydrology models.

Anthropogenic effects and sea level contributions. Another application of these water storage estimates as a stand-alone product is the general issue of hydrological contributions to sea level change: what regions are important contributors, and at what time scales? The results shown in Figure 9, for example, can be loosely interpreted as the contribution to global sea level change from those river basins (after scaling by the ratio of the land area to the area of the ocean, and reversing the sign). Though the connection is not that simple, of course, since the water that leaves a river basin does not necessarily go directly into the ocean.

The variability evident in Figure 9 is mostly seasonal. Of more relevance to the issue of rising sea level, would be regions that display linear trends. Trends can be an indication of anthropogenic influence. Groundwater is particularly susceptible to anthropogenic changes, both negative and positive; e.g. aquifer pumping to obtain water for agricultural and urban use, and groundwater infiltration from irrigation. Because few large-scale land surface models include groundwater storage, and fewer still include anthropogenic effects, contributions such as these can not be extracted from models. Time-variable satellite gravity measurements offer a means of monitoring this variability (Boy and Chao, 2002; Rodell and Famiglietti, 2002).

Precipitation (P) minus evapotranspiration (ET). P and ET have an important impact on climate, because their difference largely determines the exchange of mass and latent heat between the atmosphere and underlying Earth. Estimates of $P - ET$ can be obtained from atmospheric models using moisture flux convergence parameters (e.g. Trenberth, *et al.*, 2006). Alternatively, for a land surface (hydrology) model P and ET are typically computed using a water and energy balance approach (Roads *et al.*, 2003). These models are the best available tools for making long-range predictions of both natural and anthropogenic climate variability. However, because of the difficulty of obtaining relevant measurements using traditional methods, it has proven difficult to assess these model components, particularly at the synoptic scales that characterize the most energetic atmospheric disturbances. At seasonal and longer time periods it is often assumed that storage changes are negligible, and that therefore $P - ET$ should balance the discharge. A model's ability to achieve this balance is sometimes used to assess the accuracy of its $P - ET$ estimates (Gutowski *et al.*, 1997; Roads, 2002). But water storage changes certainly do exist (see Figures 2b, 8, and 9, for example), and at seasonal periods are typically of the same order as the discharge.

Time variable gravity offers a new opportunity for determining $P - ET$ (see Rodell *et al.*, 2004b; Swenson and Wahr, 2006b). The water budget equation is

$$dS/dt = P - ET - R, \tag{25}$$

where S is total water storage and R is discharge. Time-variable gravity measurements can be used to estimate S in a river basin. If the river that drains that basin is gauged, then the discharge can be measured and so $P - ET$ can be determined. As an example, the bottom panel of Figure 10 (provided by Sean Swenson) compares $P - ET$ estimates for the Ob River in Siberia from GRACE and river discharge, with atmospheric model estimates from ECMWF and NCEP. Clearly these models do a good job at reproducing $P - ET$ in this basin.

As a variation of this application, suppose atmospheric models are believed to accurately predict $P - ET$ within some river basin. Time-variable gravity estimates of S can then

be used in (25), along with the $P - ET$ results, to estimate the river discharge (Syed *et al.*, 2005). This offers a means of determining discharge for rivers that are not adequately gauged.

3.2 Cryosphere

One of the most important likely consequences of rising global temperatures is increased global sea levels caused by accelerated mass loss of the Antarctic and Greenland ice sheets. There is enough frozen water in those ice sheets to raise the world's oceans by 70 meters if they melted completely. Even a relatively small change in ice mass could thus have a significant impact on sea level. There have been recent, significant improvements in ice sheet monitoring, using a variety of techniques, including radar- and laser-altimeter measurements of changes in ice sheet elevations, radar-based measurements of the velocities and thinning rates of outlet glaciers, and ground-based mass balance studies that compare accumulation with discharge and melting (e.g. Church *et al.*, 2001; Rignot and Thomas, 2002; Davis et al., 2005; Zwally *et al.*, 2005; Rignot and Kanagaratnam, 2006). The conclusions of different studies are not always in good agreement. Improved monitoring of ice sheet variability would help in understanding the present mass imbalance of the ice sheets, and could significantly improve predictions of future change.

Time-variable gravity provides a method of monitoring changes in ice sheet mass that is not only independent of other methods, but that is arguably the most promising method for estimating the mass imbalance of an entire ice sheet. There have already been several GRACE estimates for Antarctica and Greenland (Velicogna and Wahr, 2005, 2006a, 2006b; Chen *et al.*, 2006b, 2006c; Luthcke *et al.*, 2006). Satellite gravity has two distinct advantages over other techniques. First, gravity measurements provide a direct estimate of mass, which is obviously the most relevant quantity for understanding mass imbalance. Other methods do not determine mass loss directly, but rely on independent assumptions to relate measured quantities to mass. Second, gravity signals at the altitude of a satellite are determined by mass variations averaged over a broad region of the underlying surface, not just at the point directly beneath the satellite. Thus, satellite gravity inherently averages over large regions. Other methods tend to sample an ice sheet at relatively small, often non-overlapping footprints, so that their estimates of total mass imbalance are subject to interpolation and extrapolation errors.

Time-variable gravity has its weaknesses, of course, For one thing, it cannot provide small-scale resolution, and so has trouble isolating the exact location of a mass anomaly. For another, time-variable gravity estimates are particularly sensitive to PGR errors. Both Antarctica and Greenland experienced significant melting at the end of the last ice age, and the underlying Earth is still rebounding. This rebound affects altimeter estimates of ice sheet thickness change: if the crust rises (or falls), the ice sheet's surface will rise (fall) along with it, and so the altimeter data will imply the ice sheet is getting thicker (thinner). It affects satellite gravity estimates because it produces a gravity signal that is inseparable from the gravity signal caused by the ongoing ice change. Because rock in the upper mantle is 3-4 times as dense as ice, PGR's relative impact on gravity is 3-4 times as large as its impact on altimeter estimates. If the Earth's surface uplifts by 1 cm, the altimeter sees the ice sheet surface rise by 1 cm. But a gravity measurement sees a gravity signal that is the equivalent of the signal from 3-4 cm of ice. Thus, although PGR models are usually used to

remove the PGR signals from both altimeter and gravity measurements, any residual errors in those models cause more problems for gravity than for altimetry. Ultimately, the best approach will be to combine time-variable gravity and altimeter estimates, as well as GPS observations of vertical crustal motion where available, to reduce the PGR errors in both techniques (Wahr *et al.*, 2000; Velicogna and Wahr, 2002).

3.3 Solid Earth

Although the Earth's mean gravity field is caused almost entirely by mass within the solid Earth, changes in the distribution of that mass generally occur too slowly, or produce gravity signals that are too small or too localized, to be practical targets of time variable satellite gravity studies. The most notable exception is PGR. The PGR signal over Canada is already clearly visible in the four years of GRACE data presently available, and has proven useful in helping to constrain the Earth's viscosity profile (Tamisiea and Davis, 2006; Paulson, *et al.*, 2007). Figure 11a, for example, shows the best-fitting linear trend in surface mass, smoothed with a 400 km Gaussian. Figure 11b shows the expected PGR signal over that same region, computed using the ICE-5G ice deglaciation model and VM2 viscosity profile (Peltier, 2004). There is clearly excellent agreement with the GRACE observations over Hudson Bay, as evidenced in Figure 11c which shows that after removing the ICE-5G results from GRACE the GRACE Hudson Bay anomaly almost completely disappears. The remaining negative anomaly over southern Alaska has been interpreted as the effects of shrinking glaciers (Tamisiea *et al.*, 2005; Chen *et al.*, 2006d).

PGR signals in Scandinavia, Antarctica, and Greenland are, as expected, proving harder to recover using GRACE, due to the problems of separating those signals from other sources of gravity trends: present-day ice mass variability within Antarctica and Greenland, and long-period hydrological and oceanographic signals in Scandinavia and northern Europe. A longer data span will improve the recovery in both Scandinavia and Canada, by averaging out more of the competing hydrological and oceanographic signals in those regions. For Antarctica and Greenland, the PGR signals can be recovered by combining time-variable gravity with ice sheet altimetry and GPS observations, as mentioned above (Wahr *et al.*, 2000; Velicogna and Wahr, 2002).

Other solid Earth applications are possible, though most likely in the form of isolated events. A good example is the 2004 Sumatran Earthquake, an event that was (of course) unexpected, but with an associated signal that is clearly evident in GRACE data (see, e.g., Han *et al.*, 2006b). This was an unusually energetic earthquake. Nevertheless, its presence in the GRACE data raises the possibility of using time-variable satellite gravity to look not only at co-seismic events, but also to search for post-seismic signals. The recovery of such signals would depend not only on the accuracy of the measurements, but also on how well the contamination from hydrological and oceanographic gravity signals can be reduced.

There is, in addition, an indirect way in which time-variable satellite gravity measurements can contribute to solid Earth studies. Global Positioning System (GPS) observations are widely used to monitor tectonic displacements of the Earth's surface. But the Earth's surface can deform in response to surface loading, as well. Load deformation is a source of noise for tectonic applications. It can be especially troublesome for campaign-style GPS observing programs, in which a site might be occupied for a few days, and then not re-occupied for perhaps several years. In that situation, seasonal and other short-period loading can alias

into apparent long-term variability.

Time-variable satellite gravity observations can be used to model and remove the large-scale component of the load deformation, and so to reduce this source of noise. The surface mass variability recovered from those observations can be convolved with solid Earth Green's functions to estimate the loading. Preliminary studies using GRACE data are described by Davis *et al.* (2004), van Dam *et al.* (2006), and King *et al.* (2006).

3.4 Oceanography

The time-variable mass signal in the ocean is small compared to that from land, as can be seen for the annual cycle from Figure 2b. Bottom pressure variability is not dominated by an annual signal to the same extent as land water storage. But even when all temporal variations are included, ocean mass fluctuations are still relatively small. Figure 12, for example, shows that the rms surface mass variability over the oceans, smoothed with a 750-km Gaussian, is typically only 2-3 cm or less. Presumably the large red regions along coastlines mostly reflect the effects of the much larger land water signals leaking into the ocean estimates. This illustrates the danger of using time-variable gravity to study the ocean near the coast. This leakage can be reduced by decreasing the smoothing radius. But a smaller radius leads to more inaccurate estimates, which makes it harder to recover the relatively small ocean signal.

Still, ocean mass signals are clearly evident in GRACE data. For example, one of the direct oceanographic applications of these mass estimates is to combine them with sea surface height measurements from altimetry, to separately estimate steric and non-steric contributions to sea surface variability. A satellite radar altimeter monitors sea surface heights along its ground-track. Suppose the altimeter detects a sea surface rise in some region. The altimeter data can not determine whether the rise was due to increased water mass in the region, or whether it was due to the water becaming warmer (and/or less salty) and expanding. Change in volume (i.e. "steric" changes) do not cause a change in gravity. Thus, satellite gravity measurements detect only the non-steric contributions. The steric contributions are then the difference between the altimeter and time-variable gravity results.

Figure 13 (results provided by Don Chambers, personal communication) shows how well this technique works on a global and seasonal scale (see, also, Chambers *et al.*, 2004; Chambers 2006a,b; Garcia *et al*, 2006). The red curve is the total ocean mass deduced from GRACE. The blue curve shows an altimetric estimate of sea surface height, corrected for steric effects using temperature and salinity profiles collected from in situ data. The altimetric and steric signals are the long-term seasonal averages of data extending well back before the launch of GRACE. Thus, the blue curve does not show actual results for 2002.5-2004.5, but shows only the best-fitting seasonal cycle, as fit to a decade or more of prior data. Even so, the agreement is excellent.

If the time-variable steric signal can be estimated for some region by differencing altimeter and mass results, it is possible to recover changes in the heat content of that region, as

$$\Delta H = \frac{\rho c_p}{\alpha}\Big(\Delta\eta - \frac{1}{\rho_0}\Delta\sigma\Big), \tag{26}$$

where ΔH is the change in ocean heat storage, ρ is the ocean density, c_p and α are the heat capacity and thermal expansion coefficient of sea water, $\Delta\sigma$ is the change in mass estimated

from time-variable gravity, and $\Delta\eta$ is the change in sea surface height measured by the altimeter (Jayne *et al.*, 2003). This result, which extends the methodology of *Chambers et al.* (1997) to include mass variability, assumes that α is independent of depth, and that the effects of salinity variations are either negligible or can be independently modeled and removed.

The exchange of heat between the ocean and atmosphere is one of the most significant examples of energy transfer within the Earth's climate system. Because of the large heat capacity of water, the ocean can store enormous amounts of energy. Therefore, it can act not only as a moderator of climate extremes, but also as an energy source for severe storms. Knowledge of the ocean's time-varying heat storage is of considerable importance for such things as climate change prediction, long-range weather forecasting, and hurricane strength prediction. Despite its great importance in climate, the ocean's time-varying heat content is greatly under-sampled because of the sparse coverage of in-situ observations. Therefore, accurate satellite mapping of the ocean's time-varying heat storage would be attractive for its global and repeating coverage.

Time-variable mass estimates can be used for other types of oceanographic applications, as well. Surface mass anomalies, $\Delta\sigma$, are proportional to variations in ocean bottom pressure

$$\Delta P_{bott}(\theta,\phi) \;=\; g\Delta\sigma(\theta,\phi) \tag{27}$$

where $\Delta\sigma$ (7) is integrated from the bottom of the ocean to the top of the atmosphere. Thus, time-variable gravity over the ocean provides estimates of sea floor pressure variability at the spatial and temporal resolution of the gravity measurements. GRACE, for example, can provide monthly sea floor pressure maps at scales of several hundred km and greater. These can be used to assess and improve oceanographic models (Condi and Wunsch, 2004; Bingham and Hughes, 2006; Zlotnicki *et al.*, 2006), and to compare with measurements from bottom pressure recorders (Kanzow *et al.*, 2005; Morison *et al.*, 2007) to separate the effects of regional and local signals.

The bottom pressure estimates can also be combined with the geostrophic assumption (which assumes a balance between pressure and Coriolis forces) to determine changes in deep ocean velocities at the temporal and spatial resolutions of the gravity field observation. For GRACE, this means the results are averaged over scales of several hundred km or more. This large a spatial scale can make it difficult to apply the geostrophic assumption at the sea floor in the presence of short-scale topography. However, simulations (Wahr *et al.*, 2002) have shown that pressure variability at the sea floor is about the same as at 2 km depth, or at even shallower depths in many cases. Thus the inferred currents can be interpreted to a high degree of accuracy in terms of the variability of currents at 2 km depth.

4 Summary

Although Satellite Laser Ranging has been providing time-variable gravity measurements for several decades, it is the much higher spatial resolution now available from GRACE that permits the kinds of applications described in this paper. The figures shown here are computed using the GRACE gravity fields available at the time of this writing (Fall, 2006). The fields will continue to improve as processing methods mature and background geophysical models get better. Any such future improvements will be retroactively applied

to all the fields, through reprocessing of the entire data set. In addition, as the GRACE time series lengthens it will become easier to separate different geophysical signals. Only with a long time series, for example, will it be possible to clearly distinguish between multi-year variability and true secular signals.

GRACE, of course, has a finite lifetime; it was designed for a 5 year mission but may last on the order of a decade. Plans for a next-generation mission are presently being formulated and assessed (Watkins *et al.*, 1998; 2000). The use of laser tracking for better monitoring the inter-satellite distance, and the introduction of a drag-free propulsion system to reduce atmospheric drag at lower altitudes, could lead to order-of-magnitude improvements in measurement accuracy. This would increase the spatial resolution even further, down to perhaps $\sim$100 km, and would enable a whole new class of applications.

5 References

Andersen O.B., Hinderer J. (2005) Global inter-annual gravity changes from GRACE: Early results. Geophys. Res. Lett., 32 (1), L01402.

Andersen O.B., Seneviratne S.I., Hinderer J., et al. (2005) GRACE-derived terrestrial water storage depletion associated with the 2003 European heat wave. Geophys. Res. Lett., 32 (18), L18405

Benjamin, D., J. Wahr, R.D. Ray, G.D. Egbert, and S.D. Desai (2006). Constraints on Mantle Anelasticity From Geodetic Observations, and Implications for the J_2 Anomaly. Geophys. J. Int., 165, 3-16.

Bingham R.J., Hughes C.W. (2006) Observing seasonal bottom pressure variability in the North Pacific with GRACE. Geophys. Res. Lett., 33 (8), L08607.

Boy J.P. and Chao B.F. (2002) Time-variable gravity signal during the water impoundment of China's Three-Gorges Reservoir. Geophys. Res. Lett., 29 (24), 2200.

Chambers D.P. (2006a) Evaluation of new GRACE time-variable gravity data over the ocean . Geophys. Res. Lett., 33 (17), L17603.

Chambers, D.P. (2006b) Observing seasonal steric sea level variations with GRACE and satellite altimetry *J. Geophys. Res. - Oceans, 111,* 3010, doi: 10.1029/2005JC002914.

Chambers, D.P., B. D. Tapley and R. H. Stewart (1997) Long-period ocean heat storage rates and basin-scale heat fluxes from TOPEX *J. Geophys. Res. - Oceans, 102,* 10,525-10,533.

Chambers, D.P., J. Wahr, and R.S. Nerem (2004) Preliminary observations of global ocean mass variations with GRACE, Geophys. Res. Lett., 31, L13310, doi:10.1029/2004GL020461.

Chao, B.F. (1994) The geoid and Earth rotation, in *Geoid and Its Geophysical Interpretations*, edited by P. Vanicek and N. Christou, pp. 285-298, CRC Press, Boca Raton, Fla..

Chao, B.F., and R.S. Gross (1987) Changes in the Earth's rotation and low-degree gravitational field induced by earthquakes, *Geophys. J. R. Astron. Soc., 91,* 569-596.

Chao B.F. and Au A.Y. (1991) Temporal variation of the Earth's low-degree zonal gravitational field caused by atmospheric mass distribution, 1980-1988. J. Geophys. Res., 96 (B4), 6569-6575.

Chen, J.L., C.R. Wilson, K.W. Seo (2006a) Optimized smoothing of gravity recovery and climate experiment (GRACE) time-variable gravity observations. *J. Geophys. Res., 111,* B06408.

Chen, J.L., C.R. Wilson, D.D. Blankenship, *et al.* (2006b) Antarctic mass rates from GRACE. Geophys. Res. Lett., 33 (11), L11502.

Chen, J.L., Wilson C.R., and Tapley B.D. (2006c) Satellite gravity measurements confirm accelerated melting of Greenland ice sheet. Science, 313, 1958-1960.

Chen, J.L., Tapley B.D., and Wilson C.R., (2006d) Alaskan mountain glacial melting observed by satellite gravimetry . Earth Planet. Sci. Lett., 248 (1-2), 368-378.

Cheng M.K. and Tapley B.D. (1999) Seasonal variations in low degree zonal harmonics of the Earth's gravity field from satellite laser ranging observations. J. Geophys. Res., 104 (B2), 2667-2681.

Cheng, M. and B.D. Tapley (2004) Variations in the Earth's oblateness during the past 28 years, *J. Geophys. Res., 109*, B09402.

Cheng, M., R. Eanes, C. Shum, B. Schutz, and B. Tapley (1989) Temporal variations in low degree zonal harmonics from Starlette orbit analysis, *Geophys. Res. Lett., 16,* 393-396.

Cheng M.K., Shum C.K. and Tapley B.D. (1997) Determination of long-term changes in the Earth's gravity field from satellite laser ranging observations. J. Geophys. Res., 102 (B10), 22377-22390.

Church, J.A., *et al.* (2001) Changes in sea level, in the *Intergovernmental Panel on Climate Change, IPCC Third Assessment Report, Climate Change 2001: The Scientific Basis* (Cambridge Univ. Press, Cambridge), pp. 639-694.

Condi F. and Wunsch C. (2004) Measuring gravity field variability, the geoid, ocean bottom pressure fluctuations, and their dynamical implications. J. Geophys. Res., 109 (C2), C02013.

Cox, C. M., and B. F. Chao (2002) Detection of a large-scale mass redistribution in the terrestrial system since 1998, *Science, 297*, 831-832.

Davis J.L., Elosequi P., Mitrovica J.X., *et al.* (2004) Climate-driven deformation of the solid Earth from GRACE and GPS. Geophys. Res. Lett., 31 (24), L24605.

Davis, C.H., Y. Li, J. R. McConnell, M. M. Frey, E. Hanna (2005) Snowfall-driven growth in East Antarctic ice sheet mitigates recent sea-level rise, *Science, 308*, 5730.

Dickey, J.O., Bentley, C.R., Bilham, R., Carton, J.A., Eanes, R.J., Herring, T.A., Kaula, W.M., Lagerloef, G.S.E., Rojstaczer, S., Smith, W.H.F., van den Dool, H.M., Wahr, J.M., Zuber, M.T. (1997) Satellite Gravity and the Geosphere, National Research Council Report, National Academy Press, 112 pp..

Dickey, J.O., S.L. Marcus, O. de Viron, and I. Fukumori (2002) Recent Earth oblateness variations: Unraveling climate and postglacial rebound effects *Science*, **298**, 1975-1977.

Dong, D., R.S. Gross, and J.O. Dickey,(1996) Seasonal variations of the Earth's gravitational field: An analysis of atmospheric and oceanic tidal excitation, *Geophys. Res. Lett., 23*, 725-728.

Dziewonski, A, and D.L. Anderson (1981) Preliminary reference Earth model, *Phys. Earth Planet. Inter.*, **25**, 297-356.

Farrell, W.E., (1972) Deformation of the Earth by surface loading, *Rev. Geophys., 10*, 761-797.

Frappart F., Ramillien G., Biancamaria S., et al. (2006) Evolution of high-latitude snow mass derived from the GRACE gravimetry mission (2002-2004). Geophys. Res. Lett., 33 (2), L02501.

Garcia D., Chao B.F., Del Rio J., *et al.* (2006) On the steric and mass-induced contributions to the annual sea level variations in the Mediterranean Sea. J. Geophys. Res., 111 (C9), C09030.

Gutowski, W.J., Y. Chen, and Z. Otles (1997) Atmospheric water vapor transport in NCEP-NCAR reanalyses: comparison with river discharge in the central United States, *Bull. Amer. Meteor. Soc.*, 78, 1957-1969.

Han, D., and J. Wahr, (1995) The viscoelastic relaxation of a realistically stratified Earth, and a further analysis of postglacial rebound, *Geophys. J. Int., 120,* 287-311.

Han S.C., Jekeli C., Shum C.K. (2004) Time-variable aliasing effects of ocean tides, atmosphere, and continental water mass on monthly mean GRACE gravity field. J. Geophys. Res., 109 (B4), B04403.

Han S.C., C.K. Shum, C. Jekeli, and D. Alsdorf (2005a) Improved estimation of terrestrial water storage changes from GRACE. Geophys. Res. Lett., 32 (7), L11502. L07302.

Han S.C., C.K. Shum, C. Jekeli, et al. (2005b) Non-isotropic filtering of GRACE temporal gravity for geophysical signal enhancement Geophys. J. Int., 163, 18-25.

Han S.C., Shum C.K., Matsumoto K. (2005c) GRACE observations of M-2 and S-2 ocean tides underneath the Filchner-Ronne and Larsen ice shelves, Antarctica. Geophys. Res. Lett., 32 (20), L20311.

Han S.C., C.K. Shum, C. Jekeli (2006a) Precise estimation of in situ geopotential differences from GRACE low-low satellite-to-satellite tracking and accelerometer data. *J. Geophys. Res., 111,* B04411.

Han S.C., C.K. Shum, M. Bevis, C.Y. Kuo (2006b) Crustal dilatation observed by GRACE after the 2004 Sumatra-Andaman earthquake. *Science, 313,* 658-662.

Hinderer J., Andersen O., Lemoine F., et al. (2006) Seasonal changes in the European gravity field from GRACE: A comparison with superconducting gravimeters and hydrology model predictions. J. Geodynamics, 41 (1-3), 59-68.

Jayne, S.R., J.M. Wahr, and F.O. Bryan (2003) Observing Ocean Heat Content Using Satellite Gravity and Altimetry, *J. Geophys. Res. - Oceans, 108,* 3031, doi:10.1029/2002JC001619.

Jekeli, C., (1981) Alternative methods to smooth the Earth's gravity field, *Rep. 327*, Dep. of Geod. Sci. and Surv., Ohio State Univ., Columbus.

Jekeli, C. (1999) The determination of gravitational potential differences from satellite-to-satellite tracking, Celestial Mech. Dyn. Astron., 75, 85-100.

Kanzow T., Flechtner F., Chave A., *et al.* (2005) Seasonal variation of ocean bottom pressure derived from Gravity Recovery and Climate Experiment (GRACE): Local validation and global patterns. J. Geophys. Res., 110 (C9), C09001.

King M., Moore P., Clarke P., *et al.* (2006) Choice of optimal averaging radii for temporal GRACE gravity solutions, a comparison with GPS and satellite altimetry. Geophys. J. Int., 166 (1), 1-11.

Knudsen P., Andersen O. (2002) Correcting GRACE gravity fields for ocean tide effects. Geophys. Res. Lett., 29 (8), 1178.

Lemoine, F.G., S. C. Kenyon, J. K. Factor, R. G. Trimmer, N. K. Pavlis, D. S. Chinn, C. M. Cox, S. M. Klosko, S. B. Luthcke, M. H. Torrence, Y. M. Wang , R. G. Williamson, E. C. Pavlis, R. H. Rapp, and T. R. Olson (1998) The development of the joint NASA GSFC and NIMA geopotential model EGM96 Goddard Space Flight Center. NASA/TP-1998-20681.

Luthcke, S.B., *et al.* (2006) Recent Greenland ice mass loss by drainage system from satellite gravity observations. Science, 10.1126/science.1130776.

Moore P., Zhang Q., and Alothman A. (2005) Annual and semiannual variations of the Earth's gravitational field from satellite laser ranging and CHAMP. J. Geophys. Res., 110 (B6), B06401.

Morison, J., Wahr, J., Kwok, R., and Peralta-Ferriz, C. (2007) Recent trends in Arctic Ocean mass distribution revealed by GRACE. submitted to *Geophys. Res. Lett.*.

Nakaegawa T. (2006) Detectability assessment of interannual variations in terrestrial water storage from satellite gravimetry using an offline land surface model simulation. Hydrological Processes, 20 (6), 1347-1364.

Nerem R.S., Eanes R.J., Thompson P.F., Chen J.L. (2000) Observations of annual variations of the Earth's gravitational field using satellite laser ranging and geophysical models. Geophys. Res. Lett., 27 (12), 1783-1786.

Neumeyer J., Barthelmes F., Dierks O., *et al.* (2006) Combination of temporal gravity variations resulting from superconducting gravimeter (SG) recordings, GRACE satellite observations and global hydrology models. J. Geodesy, 79 (10-11), 573-585.

Niu G.Y., Yang Z.L. (2006) Assessing a land surface model's improvements with GRACE estimates. Geophys. Res. Lett., 33 (7), L07401.

Paulson, A., S. Zhong, and J. Wahr (2007) Inference of mantle viscosity from GRACE and relative sea level data, submitted to *Geophys. J. Int.*.

Peltier, W.R. (2004) Global Glacial Isostasy and the Surface of the Ice-Age Earth: The ICE-5G(VM2) model and GRACE, *Ann. Rev. Earth Planet. Sci.*, **32**, 111-149.

Ramillien G., Cazenave A., Brunau O. (2004) Global time variations of hydrological signals from GRACE satellite gravimetry. Geophys J. Int., 158 (3), 813-826.

Ramillien G., Frappart F., Cazenave A., et al. (2005) Time variations of land water storage from an inversion of 2 years of GRACE geoids. Earth Planet. Sci. Lett., 235 (1-2), 283-301.

Ray, R. and Luthcke, S. (2006) Tide model errors and GRACE gravimetry, Geophys. J. Int. (in press).

Reigber C., Luhr H. and Schwintzer P. (2002) CHAMP mission status. Advances in Space Research, 30 (2), 129-134.

Rignot, E., and R. Thomas (2002) Mass balance of polar ice sheets, *Science, 297*, 1502.

Rignot, E. and P. Kanagaratnam (2006) Changes in the velocity structure of the Greenland ice sheet, . *Science, 311*, 5763.

Roads, J. (2002) Closing the water budget, *GEWEX NEWS*, 12(1), 1-6.

Roads, J., et. al. (2003) GCIP water and energy budget synthesis (WEBS). *J. Geophys. Res.*, 108(16), 8609,
doi:10.1029/2002JD002583.

Rodell M., Famiglietti J.S. (2002) The potential for satellite-based monitoring of groundwater storage changes using GRACE: the High Plains aquifer, Central US. J. Hydrology, 263 (1-4), 245-256.

Rodell, *et al.* (2004a) The Global Land Data Assimilation System, *Bull. Amer. Met. Soc., 85*, 381-394.

Rodell, *et al.* (2004b) Basin scale estimates of evapotranspiration using GRACE and other observations,

Rowlands D.D., S.B. Luthcke, S.M. Klosko SM, *et al.* (2005) Resolving mass flux at high spatial and temporal resolution using GRACE intersatellite measurements. Geophys. Res. Lett., 32 (4), L04310.

Rubincam, D.P., (1984) Postglacial rebound observed by Lageos and the effective viscosity of the lower mantle, *J. Geophys. Res., 89*, 1077-1088.

Schmidt M., Han S.C., Kusche J., et al. (2006a) Regional high-resolution spatiotemporal gravity modeling from GRACE data using spherical wavelets. Geophys. Res. Lett., 33 (8), L08403.

Schmidt R., Schwintzer P., Flechtner F., et al. (2006b) GRACE observations of changes in continental water storage. Global Planet. Change, 50 (1-2), 112-126.

Schrama, E.J.O. (2004) Impact of limitations in geophysical background models on follow-on gravity missions. Earth Moon and Planets, 94. 143-163.

Seo, K.W., and C.R. Wilson (2005) Simulated estimation of hydrological loads from GRACE,*Journal of Geodesy*, 78, 442-456, doi 10.1007/s00190-004-0410-5.

Seo K.W., Wilson C.R., Famiglietti J.S., et al. (2006) Terrestrial water mass load changes from Gravity Recovery And Climate Experiment (GRACE). Water Resources Research, 42 (5), W05417.

Song Y.T. and Zlotnicki V. (2004) Ocean bottom pressure waves predicted in the tropical Pacific. Geophys. Res. Lett., 31 (5), L05306.

Swenson, S, and Milly, P.C.M. (2006) Climate-Model biases in seasonality of continental water storage recovered by satellite gravimetry, Water Resources Research, 42, W03201, doi:10.1029/2005WR004628.

Swenson, S, and J. Wahr (2002a) Estimated effects of the vertical structure of atmospheric mass on the time-variable geoid. J. Geophys. Res., 107 (B9), 2194, doi:10.1029/2001JB000515.

Swenson, S., and J. Wahr (2002b) Methods for inferring regional surface-mass anomalies from GRACE measurements of time-variable gravity, *J. Geophys. Res.*, 107(B9), 2193.

Swenson, S., J. Wahr, and P.C.D. Milly (2003) Estimated accuracies of regional water storage variations inferred from the Gravity Recovery and Climate Experiment (GRACE), *Water Resour. Res.*, 39(8), 1223, doi:10.1029/2002WR001808.

Swenson, S, and J. Wahr (2006a) Post-processing removal of correlated errors in GRACE data. *Geophys. Res. Lett., 33*, L08402, doi:10.1029/2005GL025285.

Swenson, S, and J. Wahr (2006b) Estimating Large-scale Precipitation Minus Evapotranspiration from GRACE Satellite Gravity Measurements, J. Hydrometeorology, 7, 252-270.

Swenson, S, P. J.-F. Yeh, J. Wahr, and J. Famiglietti (2006) A comparison of terrestrial water storage variations from GRACE with in situ measurements from Illinois, Geophys. Res. Lett., 33, , L16401.

Syed T.H., Famiglietti J.S., Chen J., et al. (2005) Total basin discharge for the Amazon and Mississippi River basins from GRACE and a land-atmosphere water balance. Geophys. Res. Lett., 32 (24), L24404.

Tamisiea M.E. and J.L. Davis (2006) Trends in the Geoid Over North America *EOS Trans. AGU, 87(36), Jt. Assem. Suppl.,* Abstract G32A-01

Tamisiea M.E., E.W. Leuliette, J.L. Davis, and J.X. Mitrovica (2005) Constraining hydrological and cryospheric mass flux in southeastern Alaska using space-based gravity measurements *Geophys. Res. Lett., 32*, L20501.

Tapley B.D., Bettadpur S., Ries J.C., *et al.* (2004a) GRACE measurements of mass variability in the Earth system Science, 305 (5683), 503-505.

Tapley B.D., Bettadpur S., Watkins M., *et al.* (2004b) The gravity recovery and climate experiment: Mission overview and early results. Geophys. Res. Lett., 31 (9), L09607.

Thompson P.F., Bettadpur S.V., Tapley B.D. (2004) Impact of short period, non-tidal, temporal mass variability on GRACE gravity estimates. Geophys. Res. Lett., 31 (6), L06619.

Trenberth, K.E., L. Smith, T. Qian, A. Dai, and J. Fasullo (2006) Estimates of the global water budget and its annual cycle using observational and model data. submitted to *J. Hydrometeorology.*

Trupin, A.(1993) Effects of polar ice on the Earth's rotation and gravitational potential. Geophys. J. Int., 113, 273-283.

Trupin, A.S., M.F. Meier, and J.M. Wahr (1992) The effect of melting glaciers on the Earth's rotation and gravitational field: 1965-1984, *Geophys. J. Int., 108*, 1-15.

van Dam, T, J. Wahr, and D. Lavallee (2006) A comparison of annual vertical crustal displacements from GPS and GRACE for sites in Europe. J. Geophys. Res. (in press).

Velicogna, I. and J. Wahr (2002) A method for separating Antarctic postglacial rebound and ice mass balance using future ICESat Geoscience Laser Altimeter System, Gravity

Recovery and Climate Experiment, and GPS satellite data. J. Geophys. Res., 107 (B10), 2263, doi:10.1029/2001JB000708.

Velicogna, I. and J. Wahr (2005) Greenland mass balance from GRACE. *Geophys. Res. Lett., 32*, L18505, doi:10.1029/2005GL023458.

Velicogna, I. and J. Wahr (2006a) Measurements of time variable gravity shows mass loss in Antarctica. *Science, 311*, 1754-1756.

Velicogna, I. and J. Wahr (2006b) Significant acceleration of Greenland ice mass loss in spring, 2004. *Nature,* doi:10.1038/nature05168.

Velicogna, I., J. Wahr, H. van den Dool (2001) Can surface pressure be used to remove atmospheric contributions from GRACE data with sufficient accuracy to recover hydrological signals? J. Geophys. Res., 106, 16,415-16,434.

Visser, P., N. Sneeuw, and C. Gerlach (2003) Energy integral method for gravity field determination from satellite orbit coordinates. Journal of Geodesy, 77, 207-216.

Wahr, J.M. and Z. Bergen (1986) The effects of mantle anelasticity on nutations, Earth tides, and tidal variations in rotation rate, *Geophys. J. Roy. Astr. Soc., 87*, 633–668.

Wahr, J., M. Molenaar, and F. Bryan, (1998) Time variability of the Earth's gravity field: Hydrological and oceanic effects and their possible detection using GRACE, *J. Geophys. Res.*, 103(B12), 30205-30229.

Wahr, J., D. Wingham, C.R. Bentley (2000) A method of combining GLAS and GRACE satellite data to constrain Antarctic mass balance, J. Geophys. Res., 105, 16,279-16,294.

Wahr, J, S.R. Jayne, and F.O. Bryan (2002) A method of inferring deep ocean currents from satellite measurements of time variable gravity. *J. Geophys. Res. - Oceans, 107*, 3218, doi:10.1029/2001JC001274.

Wahr, J., S. Swenson, and I. Velicogna (2006) The Accuracy of GRACE Mass Estimates. *Geophys. Res. Lett., 33*, L06401, doi:10.1029/2005GL025305.

Watkins M.M. *et al.* (1998) Ongoing Observations of Mass Redistribution in the Earth System: GRACE Follow-On Mission(s) Concept for an Earth Science Mission in the Post-2002 Era, submitted to the NASA Post-2002 EOS planning RFI ("Easton Workshop").

Watkins M.M., W.M. Folkner, B. Chao, and B. D. Tapley (2000) EX-5: A Laser Interferometer Follow-On to the GRACE Mission, Gravity, Geoid, and Geodynamics: IAG International Symposium GGG2000, Banff, Alberta, Canada, v. 123, M. Sideris (ed.), Springer-Verlag, New York.

Watkins, M. M., and D.N. Yuan (2006) Beyond Harmonics: Recent Mascon Solutions from GRACE. Geophysical Research Abstracts, 8, 09474, 2006; SRef-ID: 1607-7962/gra/EGU06-A-09474.

Yeh, P.J.-F., Swenson S, Famiglietti J., and Rodell M. (2006) Remote sensing of groundwater storage changes in Illinois using GRACE. Water. Res. Research (in press).

Yoder, C.F., J.G. Williams, J.O. Dickey, B.E. Schutz, R.J. Eanes, and B.D. Tapley (1983) Secular variations of Earth's gravitational harmonic $Jsub2$ coefficient from Lageos and the non-tidal acceleration of Earth rotation, *Nature, 303*, 757-762.

Yuan, D., and M.M. Watkins (2006) Recent Mascon Results from GRACE, Hotine-Marussi Symposium of Theoretical and Computational Geodesy: Challenge and Role of Modern Geodesy Wuhan University.

Zwally, J. *et al.* (2005) Mass changes of the Greenland and Antarctic ice sheets and shelves and contributions to sea-level rise: 1992-2002. *J. Glaciol., 51*, 175.

Zlotnicki, V., J. Wahr, and T. Song (2006) The Antarctic circumpolar current: seasonal transport during 2002-2004. J. Phys. Ocean. (in press).

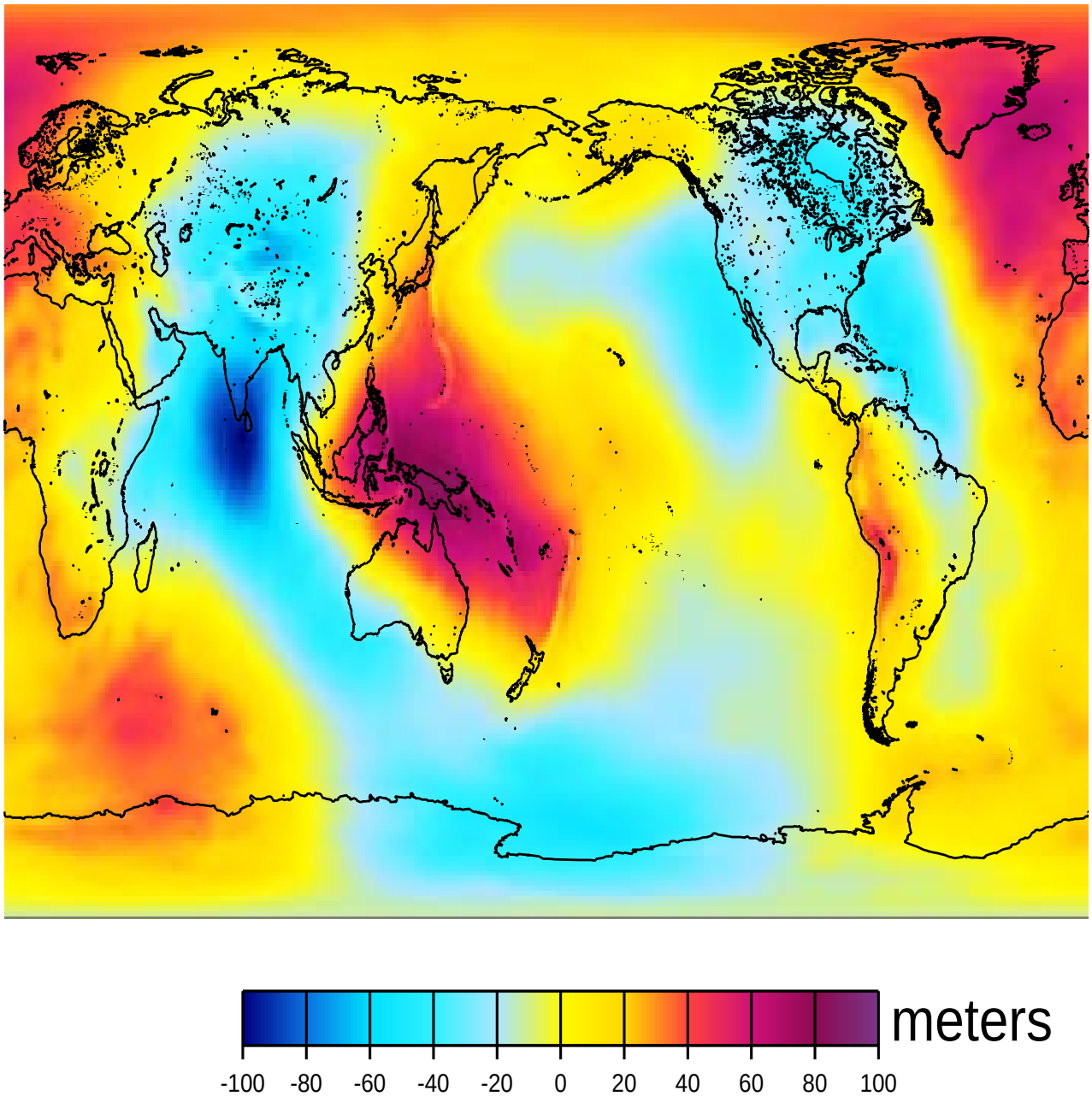

Figure 1: The time-averaged geoid anomaly from EGM96 (Lemoine et *et al.*, 1998).

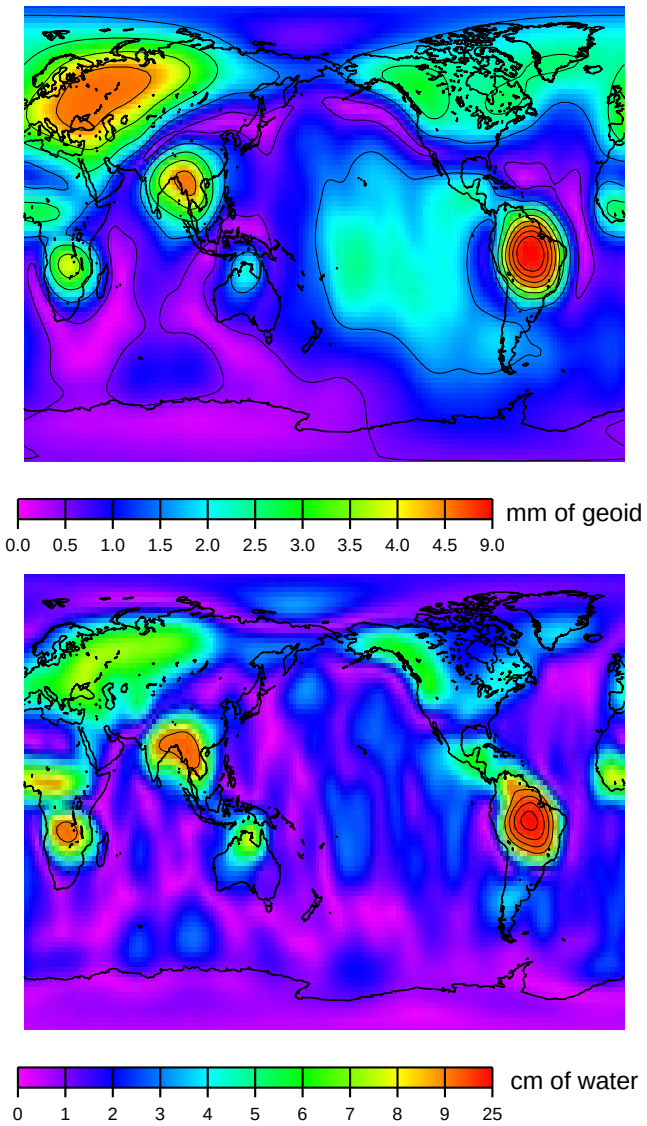

Figure 2: The top panel shows the amplitude of the annual cycle in the geoid , fit to 4 years (spring 2002 to spring 2006) of monthly gravity field solutions from GRACE. A 750-km Gaussian smoothing function has been applied to the results. The bottom panel shows the corresponding amplitude of the annual cycle in surface mass, also smoothed with a 750 km Gaussian, in units of cm of water thickness. The solid lines represent contour intervals of 1 mm in the top panel and 4 cm in the bottom panel.

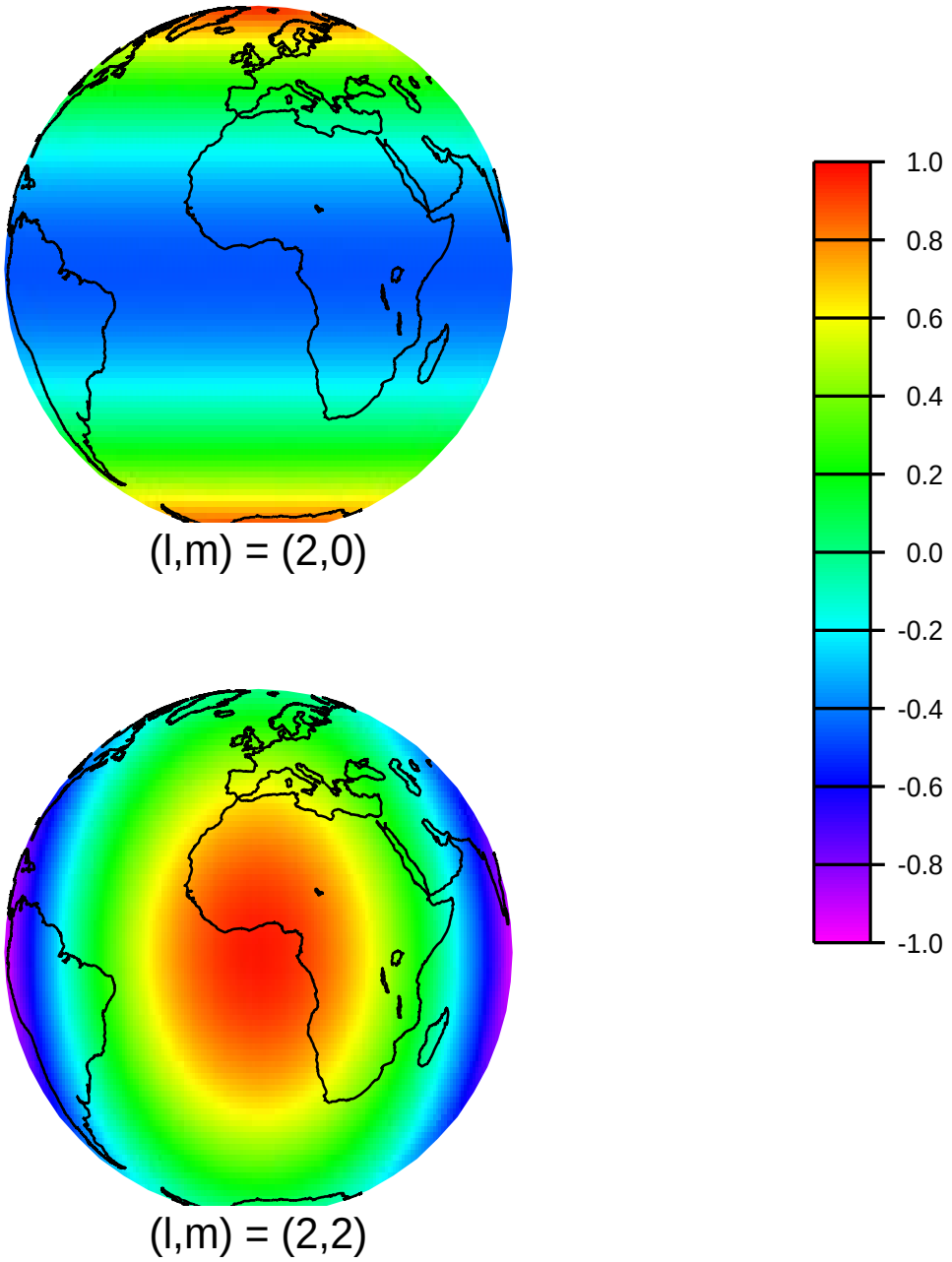

Figure 3: The spatial patterns of the Legendre functions $\tilde{P}_{20}$ and $\tilde{P}_{22}$.

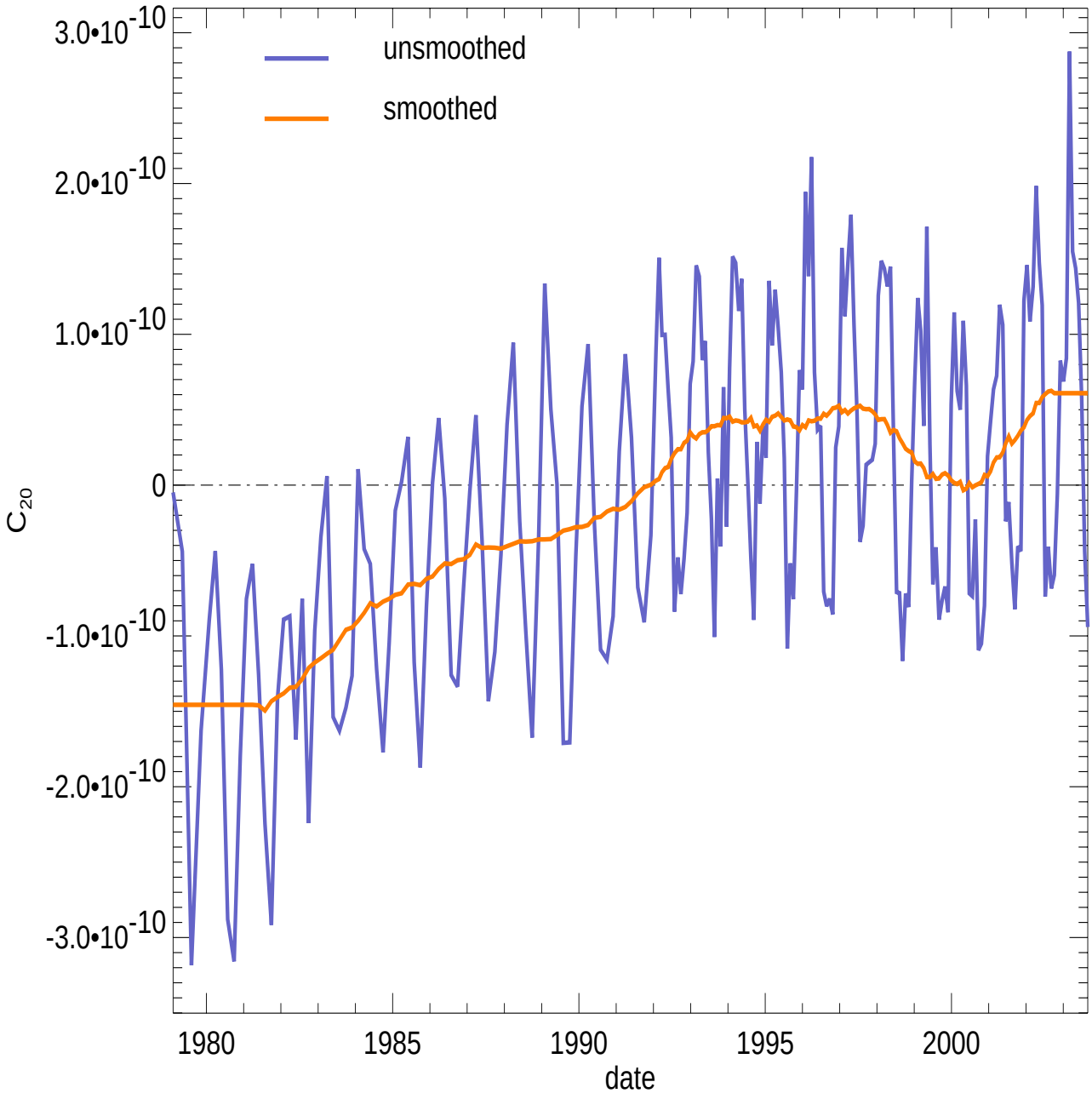

Figure 4: The blue line shows a time series of C_{20}, determined from more than 20 years of SLR measurements (data provided by Chris Cox). The red line is a smoothed version of those values, obtained by first fitting and removing seasonal terms and then applying a 23-month moving average to the residuals.

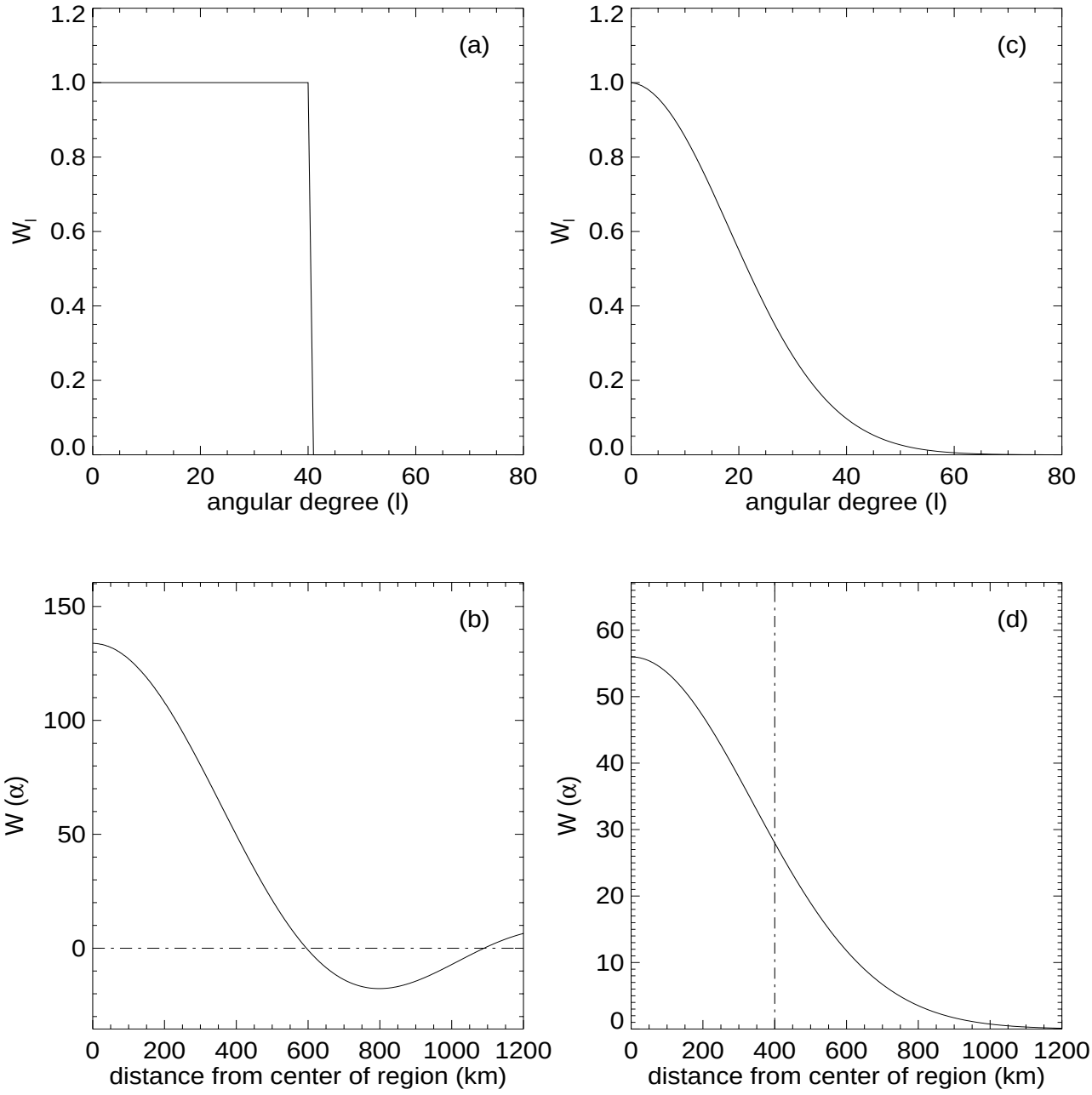

Figure 5: (a) the spectral smoothing coefficients equivalent to truncation at degree $l = 40$, and (b) the corresponding smoothing function in the spatial domain. (c) the spectral smoothing coefficients for Gaussian smoothing with a 400 km radius, and (d) the corresponding smoothing function in the spatial domain.

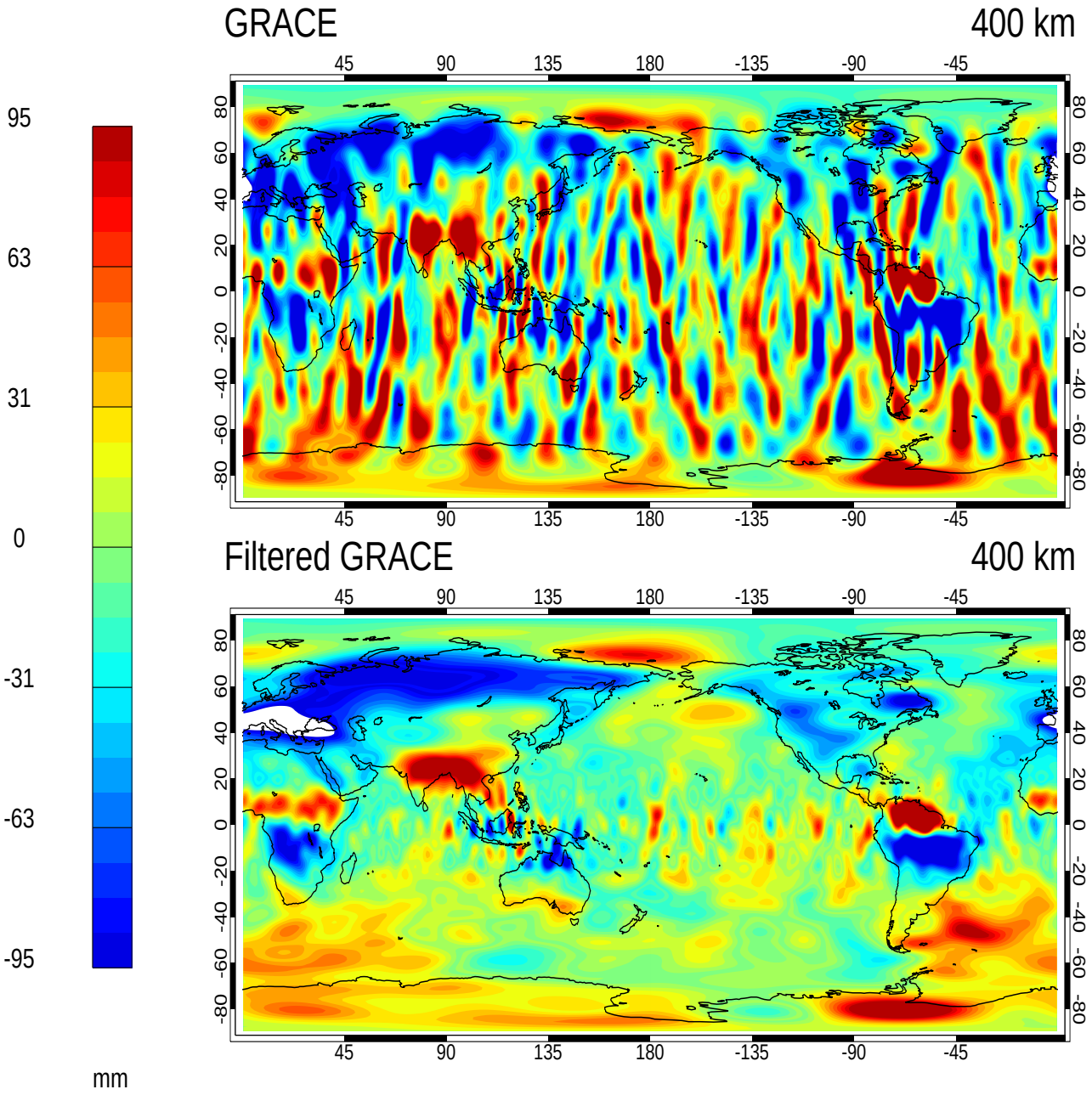

Figure 6: The top panel shows surface mass anomalies deduced from GRACE for a single month, after the temporal mean has been removed. The units are mm of water thickness. The bottom panel shows the same thing, but after post-processing the Stokes coefficients to reduce noise as described by Swenson and Wahr (2006a). (Figure provided by Sean Swenson.)

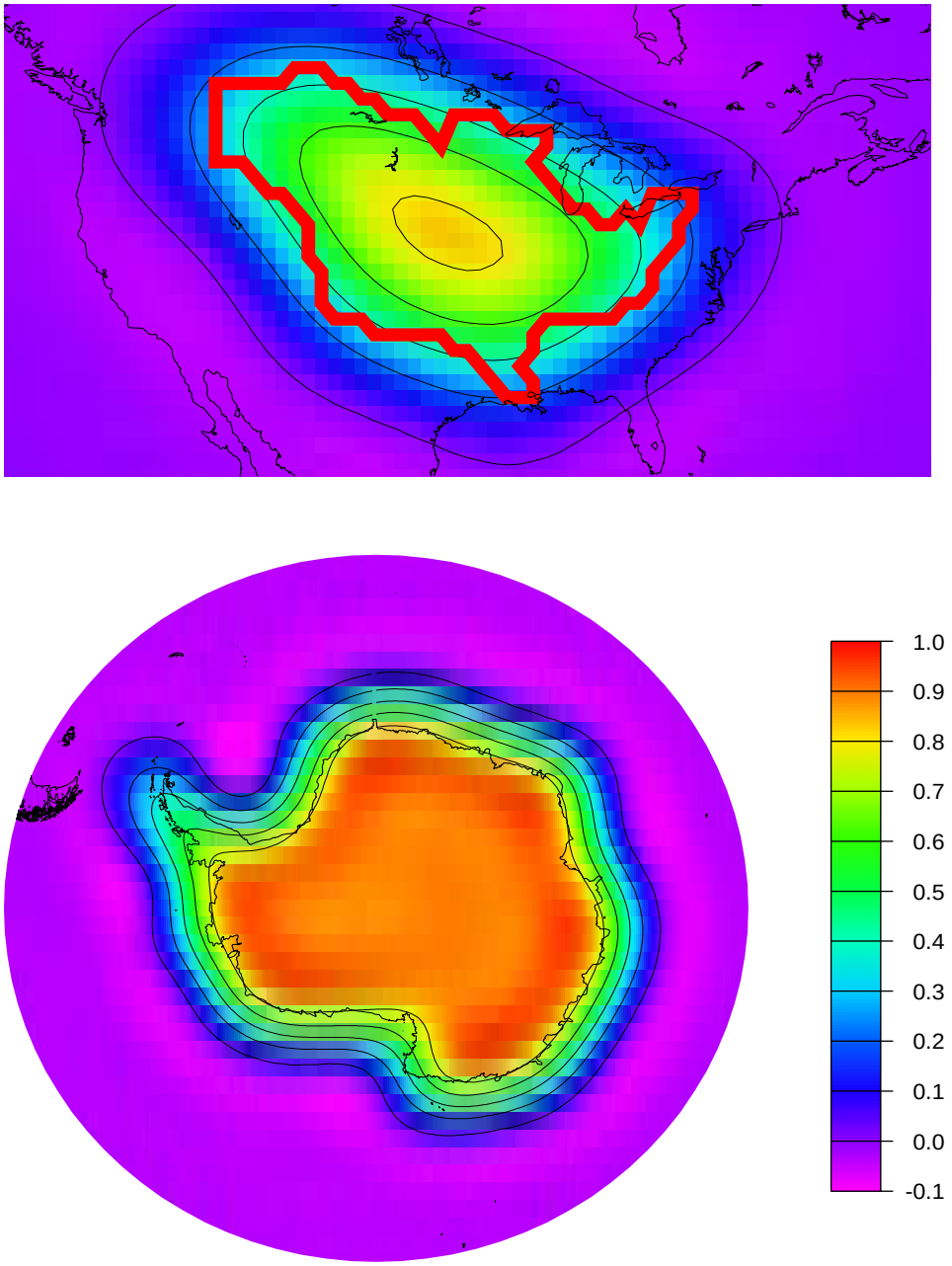

Figure 7: Averaging functions, $\overline{W}$ (see equation (21)), for the Mississippi River basin and for Antarctica. The solid lines represent contour intervals of 0.2.

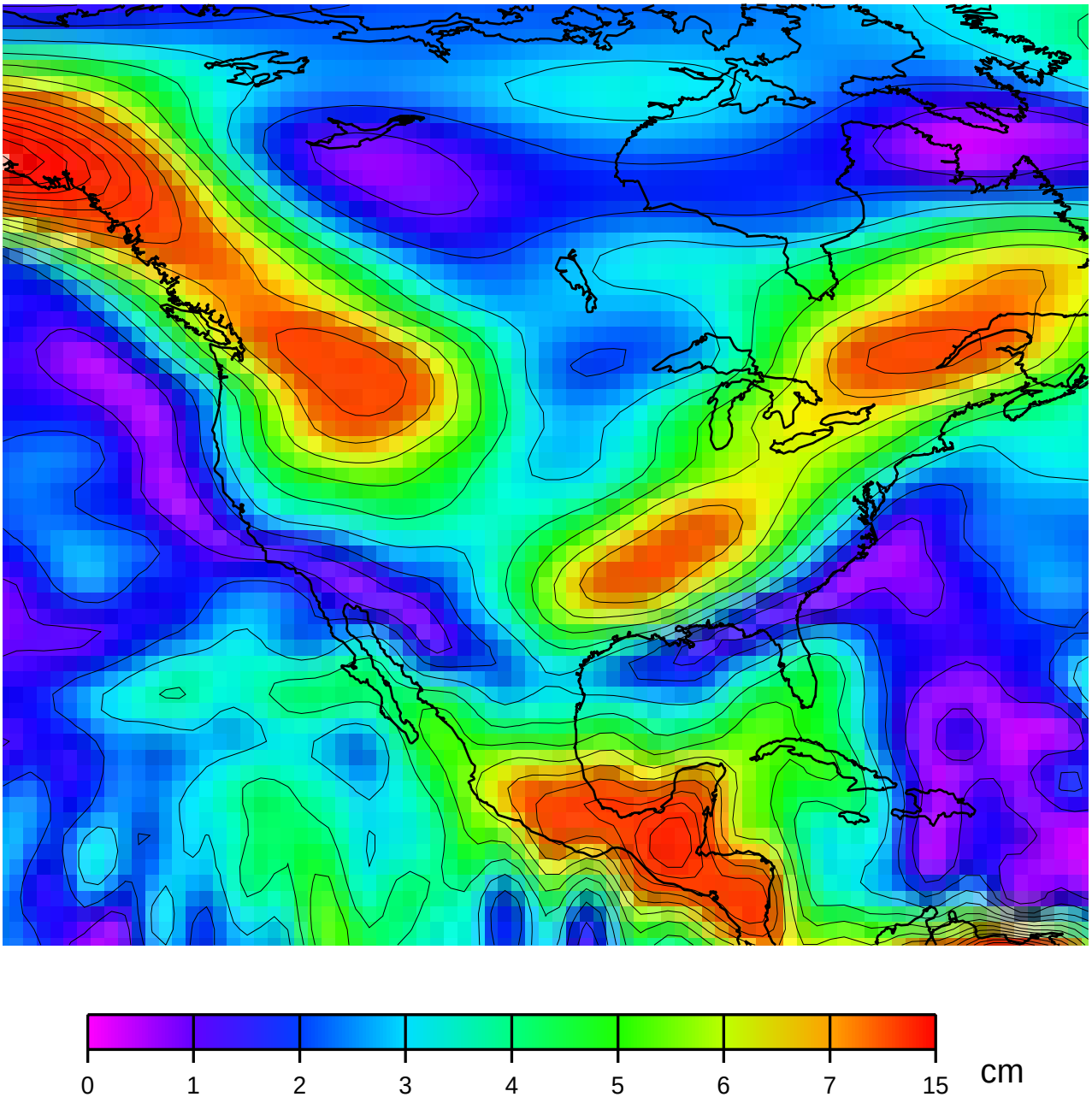

Figure 8: The amplitude of the annually varying mass signal, in units of cm of water thickness, recovered from GRACE during spring 2002 through spring 2006. The results have been post-processed to reduce noise (Swenson and Wahr, 2006a), and smoothed with a 300 km Gaussian. The solid lines represent contour intervals of 1 cm.

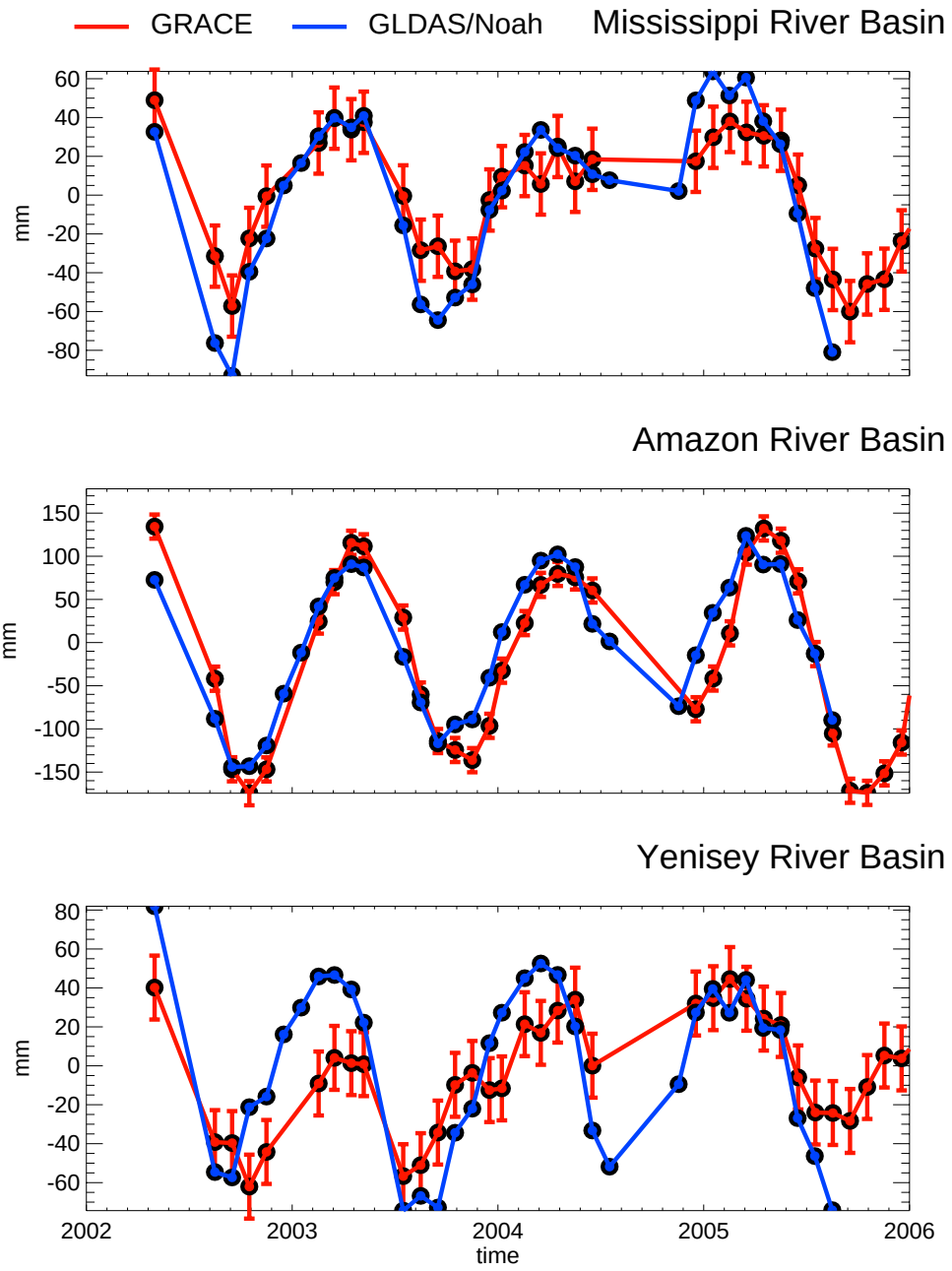

Figure 9: Water storage results for three river basins, obtained using specially constructed averaging kernels for those basins. GRACE results, with their 68.3% confidence limits, are shown in red (post-processed to reduce noise, as described by Swenson and Wahr (2006a)). Results from the GLDAS/Noah land surface model (Rodell, *et al.*, 2004) are in blue. (Figure provided by Sean Swenson.)

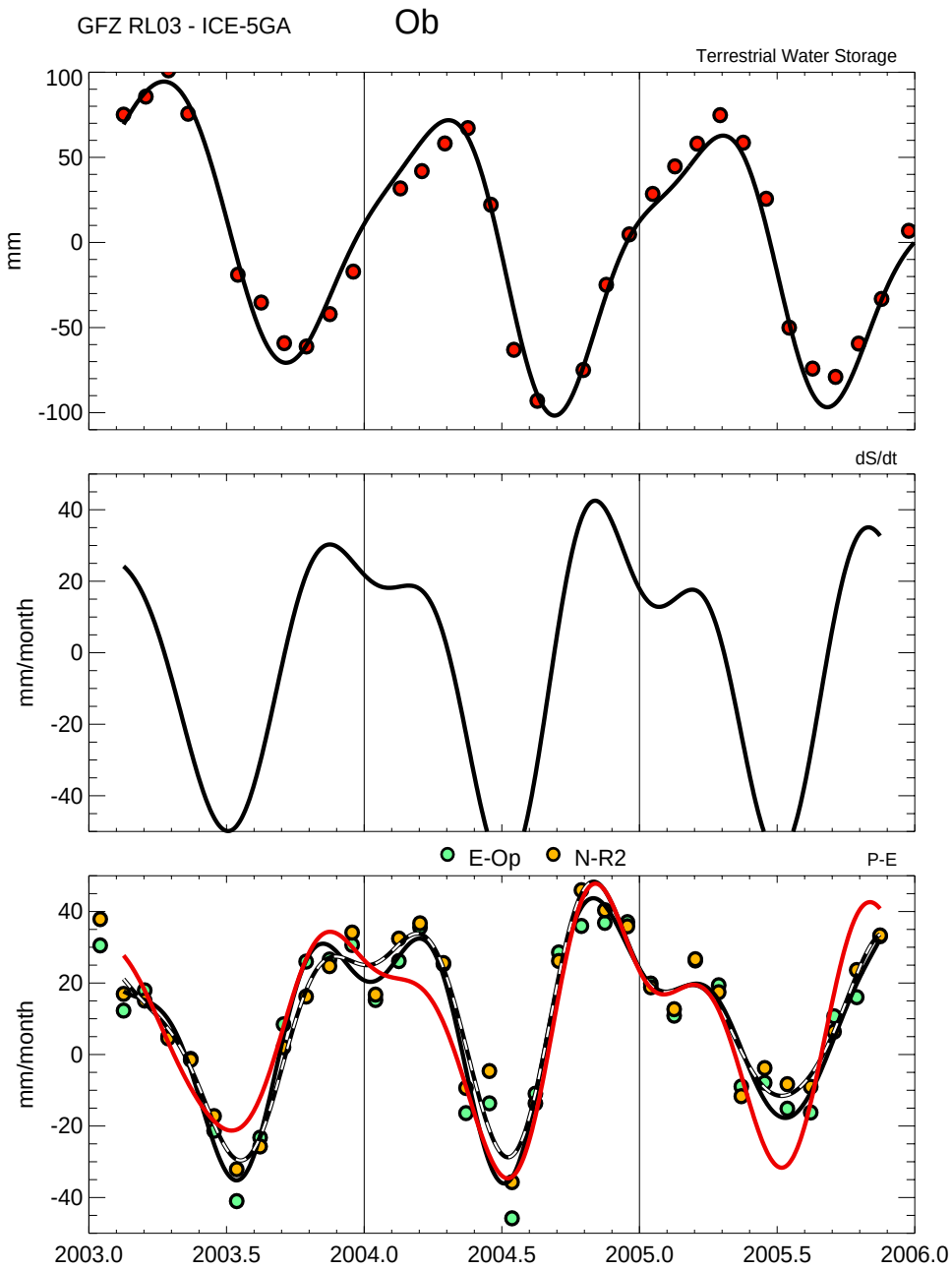

Figure 10: Top: Red dots are GRACE water storage estimates (S) for the Ob River; the black line is a smoothed version. Middle: the time derivative (dS/dt) of the smoothed water storage. Bottom: Red line is the sum of dS/dt and the measured Ob discharge (R), and so is an estimate of $P - ET$. Green and orange dots are estimates of $P - ET$, using moisture convergence parameters from the ECMWF (green) and NCEP (orange) models. Solid black and hatched black lines are smoothed version of ECMWF and NCEP, respectively. (Figure provided by Sean Swenson.)

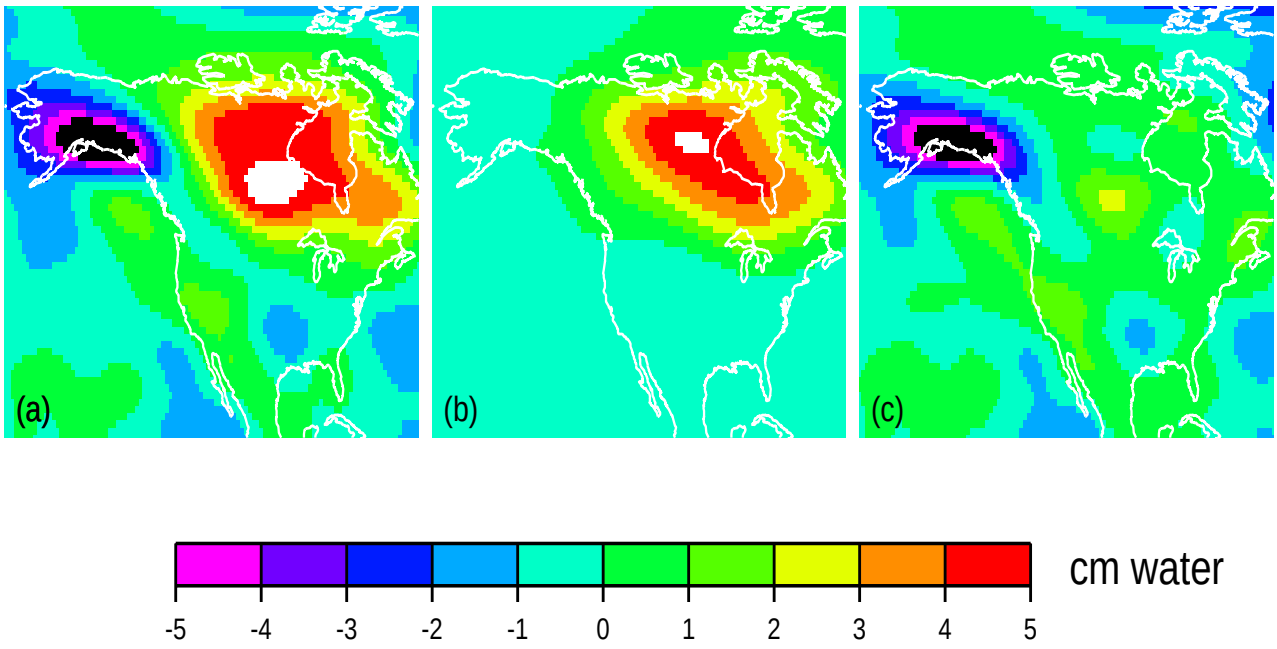

Figure 11: (a) the best-fitting linear trend for the GRACE fields between spring 2002 and spring 2004, after post-processing the fields as described by Swenson and Wahr (2006a). Results have been smoothed with a 400-km Gaussian smoothing function. Units are in cm/yr of water thickness. (b) predictions based on the ICE-5G PGR ice deglaciation model (Peltier, 2004). (c) the difference between (a) and (b).

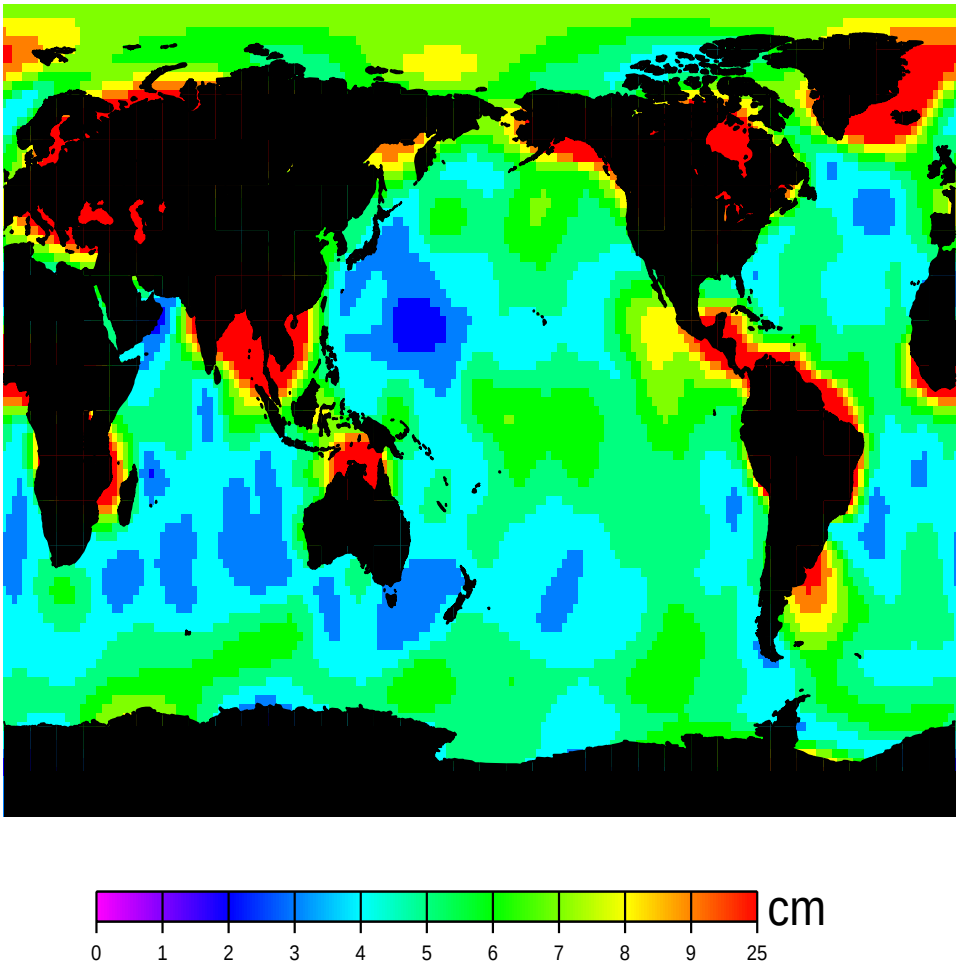

Figure 12: The rms about the mean of ocean surface mass variability deduced from GRACE for spring 2002 through spring 2006, smoothed with a 750-km Gaussian.

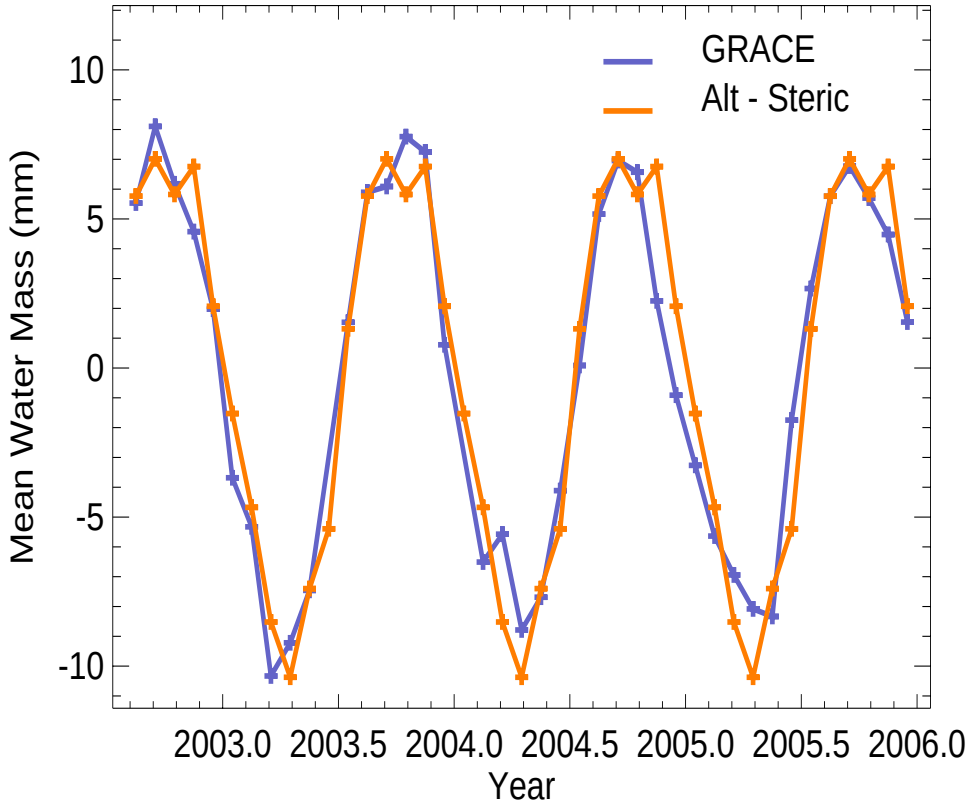

Figure 13: Compares seasonal estimates of total ocean mass from GRACE, with estimates deduced from a combination of satellite altimetry and in situ temperature and salinity measurements. (Results provided by Don Chambers).

Table 1. Elastic Love Numbers k_l Computed by Dazhong Han as described by *Han and Wahr* (1995), for Earth Model PREM (*Dziewonski and Anderson*, 1981).

l	k_l
0	+0.000
1	+0.027
2	-0.303
3	-0.194
4	-0.132
5	-0.104
6	-0.089
7	-0.081
8	-0.076
9	-0.072
10	-0.069
12	-0.064
15	-0.058
20	-0.051
30	-0.040
40	-0.033
50	-0.027
70	-0.020
100	-0.014
150	-0.010
200	-0.007

The $l = 1$ value assumes the origin of the coordinate system is the center of figure of the solid Earth's surface (see text).

:

: